Coupled Ocean-Atmosphere Variability in the Tropical Indian Ocean

Toshio Yamagata[1,2], Swadhin K. Behera[1], Jing-Jia Luo[1], Sebastien Masson[1], Mark R. Jury[3], and Suryachandra A. Rao[1]

The Indian Ocean Dipole (IOD) is a natural ocean–atmosphere coupled mode that plays important roles in seasonal and interannual climate variations. The coupled mode locked to boreal summer and fall is distinguished as a dipole in the SST anomalies that are coupled to zonal winds. The equatorial winds reverse their direction from westerlies to easterlies during the peak phase of the positive IOD events when SST is cool in the east and warm in the west. In response to changes in the wind, the thermocline rises in the east and subsides in the west. Subsurface equatorial long Rossby waves play a major role in strengthening SST anomalies in the central and western parts. The SINTEX-F1 coupled model results support the observational finding that these equatorial Rossby waves are coupled to the surface wind forcing associated with IOD rather than ENSO. The ENSO influence is only distinct in off-equatorial latitudes south of 10°S. Although IOD events dominate the ocean–atmosphere variability during its evolution, their less frequent occurrence compared to ENSO events leads the mode to the second seat in the interannual variability. Therefore, it is necessary to remove the most dominant uniform mode to capture the IOD statistically. The seasonally stratified correlation between the indices of IOD and ENSO peaks at 0.53 in September–November. This means that only one third of IOD events are associated with ENSO events. Since a large number of IOD events are not associated with ENSO events, the independent nature of IOD is examined using partial correlation and pure composite techniques. Through changes in atmospheric circulation and water vapor transport, a positive IOD event causes drought in Indonesia, above normal rainfall in Africa, India, Bangladesh and Vietnam, and dry as well as hot summer in Europe, Japan, Korea and East China. In the Southern Hemisphere, the positive IOD causes dry winter in Australia, and dry as well as warm conditions in Brazil. The identification of IOD events has raised a new possibility to make a real advance in the predictability of seasonal and interannual climate variations that originate in the tropics.

[1]Frontier Research System for Global Change, Yokohama, Kanagawa 236–0001, Japan.
[2]Department of Earth and Planetary Science, The University of Tokyo, Tokyo 113–0033, Japan.
[3]Environmental Science Department, University of Zululand, South Africa.

Book Title
Book Series

10.1029/Series#LettersChapter#

1. INTRODUCTION

Tropical oceans play major roles in the natural variability of the world climate. Anomalous coupled ocean–atmosphere phenomena generated in the tropical oceans produce global atmospheric and oceanic circulation changes that influence regional climate conditions even in remote regions. On the interannual time scale, the El Niño-Southern Oscillation (ENSO) of the tropical Pacific Ocean is known as one typi-

cal example of such phenomena and has so far received worldwide attention because of the enormous societal impact.

In contrast to the Pacific, the interannual variability originated in the tropical Indian Ocean has not been paid much attention. This is mainly because the variability in the basin is overwhelmed by seasonal winds. The southwest monsoon winds that dominate the annual cycle produce strong upwelling along the Somali coast of the western Indian Ocean. Weakening of these winds during the boreal fall after the summer monsoon period gives rise to warmer SST mainly owing to weakened upwelling. During this time, the equatorial westerly winds become stronger and generate the strong equatorial currents known as the *Yoshida-Wyrtki* jet, which transports the warm waters to the east. In some years such as 1994, however, the *Yoshida-Wyrtki* jet did not evolve in such a normal way. This was a puzzle [e.g., *Vinayachandran et al.*, 1999].

It has turned out that the 1994 anomalous event in the basin is due to an ocean–atmosphere coupled phenomenon. This coupled mode is now widely called the Indian Ocean Dipole (IOD) [*Saji et al.*, 1999; *Yamagata et al*., 2003]; it is sometimes referred to as the Indian Ocean Zonal (IOZ) mode. During these IOD/IOZ events, an east–west dipole pattern in SST anomalies evolves in tropical Indian Ocean. The changes in SST are found to be closely associated with changes in surface winds; equatorial winds reverse direction from westerlies to easterlies during the peak phase of the positive IOD events when SST is cool in the east and warm in the west. Changes in surface winds are associated with a basin-wide anomalous Walker circulation [*Yamagata et al*., 2002]. These ocean and atmosphere conditions imply that a Bjerknes-type [*Bjerknes*, 1969] feedback mechanism is responsible for the IOD evolution.

The dipole pattern is not restricted only to SST anomalies. The thermocline rises in the east and deepens in the central and western parts in response to anomalous equatorial winds during the IOD events, thus giving rise to a subsurface dipole [*Rao et al*., 2002a]. Since the seasonal southeasterly winds along the Java coast are also strengthened during the positive IOD events, the anomalous coastal upwelling causes further SST cooling in the east [*Behera et al*., 1999]. The dipole pattern related to IOD is thus observed in heat content/sea level anomalies [*Rao et al.,* 2002a]. The atmospheric component of IOD is seen in OLR anomalies [*Behera et al*., 1999, 2003a; *Yamagata et al*., 2002] and sea level pressure anomalies [*Behera and Yamagata*, 2003]. Therefore, IOD indices are derived for various ocean–atmosphere variables: SST anomalies from GISST, zonal wind anomaly from NCEP-NCAR reanalysis data, sea surface height anomaly from simple ocean data assimilation (SODA) products, sea level anomaly from TOPEX/POSEIDON data and satellite derived OLR anomaly [see Figure 1 of *Yamagata et al*., 2003].

Several other studies also discussed various aspects of this Indian Ocean coupled phenomenon [*Webster et al*., 1999; *Murtugudde et al*., 2000; *Feng et al*., 2001; *Li and Mu,* 2001; *Rao et al*., 2002b; *Vinayachandran et al*., 1999; 2002; *Xie et al*., 2002; *Saji and Yamagata,* 2003a; *Guan et al*., 2003; *Masson et al*., 2003a; *Ashok et al*., 2003a; *Annamalai et al*., 2003; *Shinoda et al*., 2003] using observed data and ocean/atmosphere model simulations. We also note that coupled general circulation models (CGCMs) are now successful in reproducing the IOD events [*Iizuka et al*., 2000; *Gualdi et al*., 2003; *Behera et al*., 2003b; *Lau and Nath,* 2004; *Cai et al*., 2003].

As expected from the practice of ENSO, the impact of the IOD is not limited only to the equatorial Indian Ocean. Through the changes in the atmospheric circulation, IOD influences the world climate [*e.g.*, *Saji and Yamagata, 2003b*]. For example, the IOD influences the Southern Oscillation in the Pacific [*Behera and Yamagata, 2003*], rainfall variability during the Indian summer monsoon [*Behera et al., 1999; Ashok et al.,* 2001], the summer climate condition in East Asia [*Guan and Yamagata, 2003; Guan et al., 2003*], the African rainfall [*Black et al.,* 2003*; Clark et al.,* 2003*; Behera et al.,* 2003b; *Rao et al.,* 2004], the Sri Lankan Maha rainfall [*Lareef et al.,* 2003] and the Australian winter climate [*Ashok et al.,* 2003b].

Discovery of the IOD has stimulated exciting research in other disciplines of science such as paleoclimate, marine biology and atmospheric chemistry. In a recent paper, *Abram et al.* [2003] reported that the scattered particulates from severe wildfires in the Indonesian region during the 1997 IOD event caused exceptional coral bleaching in the Mentawai Island (off Sumatra) reef ecosystem. They also traced the IOD signal back to the mid-Holocene period using the fossil coral records from the region, revealing the first evidence of paleo-IOD. In another context, *Fujiwara et al.* [1999] found that the variability in tropospheric ozone distribution over Indonesia is related to the IOD phenomenon.

Since the above new concept of IOD was introduced in 1999, several interesting issues related to its existence/nonexistence and dependence/independence of ENSO have been raised mostly on the basis of statistics [*e.g., Allan et al.,* 2001*; Dommenget and Latif,* 2002*; Baquero-Bernal et al.,* 2002*; Hastenrath,* 2002]. Although simple statistical analyses can capture physical modes, more sophisticated methods sometimes could be misleading if not supported by our state-of-art understanding of dynamics. In the present study, we address these issues using multiple datasets including results from a coupled model simulation. The long time series of the data derived from the coupled model simulation on the Earth Simulator improves the statistical confidence in identifying the independent evolution of IOD and its global teleconnections.

2. MODEL AND DATA

The model results used in the study are obtained from an ocean–atmosphere–land coupled general circulation model (CGCM) simulation. The CGCM known as SINTEX-F1 (SINTEX-FRSGC] is an upgraded version [*Masson et al.,* 2003b*; Luo et al.,* 2003] of the original SINTEX (Scale Interaction Experiment of EU project) model described in *Gualdi et al.* [2003]. The model is also modified in coding to adapt to the unique new-generation machine called the Earth Simulator. In this model, the atmospheric component ECHAM-4 [*Roeckner et al.,* 1996] is coupled to the ocean component OPA 8.2 [*Madec et al.,* 1998] through the coupler OASIS 2.4 [*Valcke et al.*, 2000]. The atmosphere model has a spectral triangular truncation of T106 with 19 vertical levels. The ocean model OPA8.2 of the ORCA2 grid uses the Arakawa C-grid with a finite mesh of 2° x 2° *cosine* (latitude) with increased meridional resolutions to 0.5° near the equator. The model's finite mesh is designed in a way that the North Pole is replaced by two node points over land, one on North America and the other on Asia. The model has 31 levels in the vertical. The details of the coupling strategy are reported in *Guilyardi et al.* [2001] and the model's skill to reproduce the Indian Ocean variability is found in *Gualdi et al.* [2003]. We note here that the present version of the SINTEX-F1 model differs in a number of ways from the SINTEX model reported in the *Gualdi et al.* [2003]. The spectral truncation in the atmospheric component here is T106 in contrast to T42. The ocean component includes a free surface, improved runoff parameterization, and a few enclosed seas previously absent in the model geometry [*Masson et al.*, 2003b]. In addition, a number of small changes boost up the performance of SINTEX-F1 [*Luo et al.,* 2003]. A complete intercomparison study of the two versions of the model along with other available coupled models is now under preparation. We use here the last 200 years monthly data derived from the 220 years simulation to compare with the observational data.

The observed data used in the analysis are from 1958 to 1999. Monthly anomalies of atmospheric fields are derived from the NCEP-NCAR reanalysis data [*Kalnay et al., 1996*]. SST anomalies are computed from the GISST 2.3b dataset [*Rayner et al.*, 1996]. Other ocean variables like the sea surface height and heat content are derived from the SODA [*Carton et al*., 2000]. The rainfall anomalies are derived from the gridded precipitation data [*Willmott and Matsuura*, 1995]. Following *Saji et al.* [1999], the Dipole Mode Index (DMI) is defined as the SST anomaly difference between western (50°E–70°E, 10°S–10°N) and eastern (90°E–110°E, 10°S–Eq) tropical Indian Ocean. Niño-3 index for the eastern Pacific is derived from the GISST data.

Besides simple linear statistical tools such as a composite technique and a correlation method, a partial correlation technique [e.g., *Yule*, 1907] is used to show a partial relationship between two variables while excluding influences arising from another independent variable. For example, the partial correlation between DMI and global precipitation anomalies, while excluding the influence due to the correlation between Niño-3 and precipitation anomalies [cf. *Saji and Yamagata*, 2003b], is defined as follows:

$$r_{13,2}=(r_{13} - r_{12} \cdot r_{23}) / \sqrt{(1 - r^2_{12})}\sqrt{(1 - r^2_{23})},$$

where r_{13} is the correlation between DMI and global precipitation anomalies, r_{12} is the correlation between DMI and Niño-3 index and r_{23} is the correlation between Niño-3 and global precipitation anomalies. Similarly, the partial correlation can also be obtained for Niño-3 and precipitation anomalies while excluding the influence due to the correlation between IOD and precipitation anomalies. Statistical significance of the correlation coefficients is determined by a 2-tailed "*t*-test".

We note that the low frequency variabilities of periods longer than 7 years are removed from all the datasets.

3. DOMINANT MODES OF THE INDIAN OCEAN SST VARIABILITY

3.1. The Basin-wide Mode

A basin-wide SST anomaly of almost uniform polarity is present as the most dominant interannual mode (Figure 1a) in the Indian Ocean [*Cadet*, 1985; *Klein et al.*, 1999]. We note that this basin-wide uniform mode shows a high correlation with the eastern Pacific SST anomalies. The peak correlation coefficient of 0.8 is found when the Niño-3 index leads the basin-wide uniform mode by 4 months (Figure 2). It is no wonder that most of the previous Indian Ocean studies mainly focused on the ENSO influence on SST variability in the basin [cf. *Latif and Barnett*, 1995; *Tourre and White*, 1997; *Venzke et al*., 2000]. The surface fluxes are identified as the major cause of SST changes during the Pacific ENSO events [*Venzke et al*., 2000]. The basin-wide warming (cooling) is observed after an El Niño (La Niña) peak owing to the reduced (enhanced) cloud cover and increased (decreased) solar insolation. Reduction (enhancement) in the wind speed also contributes to the warming (cooling) through changes in the latent heat flux. Therefore, it is clear that the basin-wide uniform mode is a consequence of ENSO forcing. A simple estimate shows that a change of 10 Wm^{-2} in the surface fluxes could lead to a change of 0.5°C in the SST over a period of 4 months for a typical mixed-layer of 50 m. This

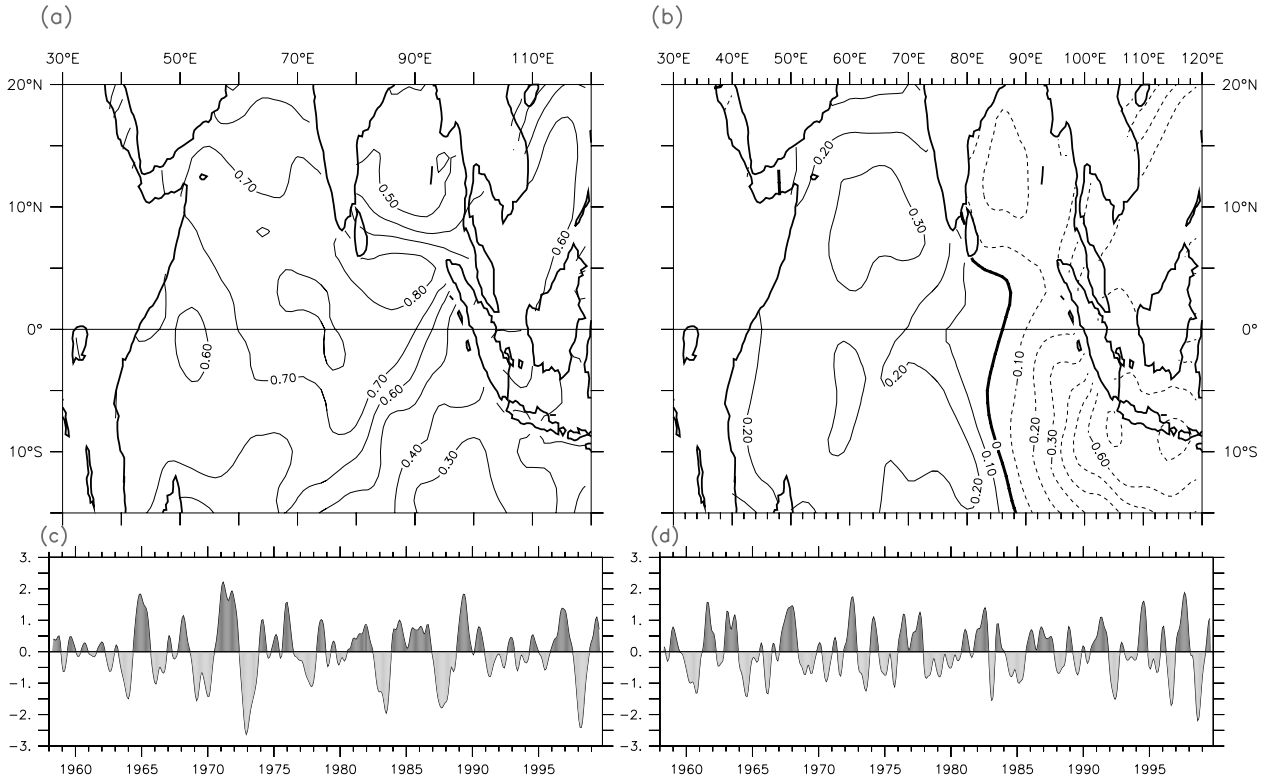

Figure 1. (a) First and (b) second EOF modes along with their respective (c and d) principal components of SST anomalies derived from GISST data.

simple estimate explains the 4 months lag in the peak correlation.

3.2. The Dipole Mode

Although IOD appears as a major signal during some years, its less frequent occurrence compared to the basin-wide uniform mode linked closely to ENSO provides IOD the second most dominant seat in the EOF analysis (Figure 1b). We also note that the period of basin-wide uniform mode is longer compared to that of the IOD mode. It is rare until now for climate dynamists to discuss the second mode of variability. This is why some researchers felt difficulties in accepting the new concept of the IOD [cf. *Allan et al*., 2001; *Hastenrath*, 2002]. Since the basin-wide uniform mode dominates the SST variability on interannual time scale, we need to filter out the externally forced mode to find the signal related to IOD in a linear statistical analysis [*Yamagata et al.*, 2003; *Behera et al.*, 2003a]. In the wavelet spectra of raw SST anomalies in the eastern pole (10°S–Eq., 90°E–110°E) and western pole (10°S–10°N, 50°E–70°E), we do not find much coherence [Figure 2 in *Yamagata et al.*, 2003]; we are apt to be misled to a denial of the dipole. However, as shown in *Yamagata et al.* [2003], a remarkable seesaw is found between the two boxes after removing the external ENSO effect (readers are referred to Figure 3 of their article). This shows quite a contrast to other major oscillatory modes such as the Southern Oscillation and the North Atlantic Oscillation. Because those are the first dominant modes even statistically, a negative correlation is observed between poles of those two modes in raw data. Since the IOD appears as the second mode statistically in SST variability, we need to remove the first dominant mode to detect its sea-saw mode statistically. This is the basic reason why some statistical analyses fail to capture the IOD signal [cf. *Dommenget and Latif*, 2002; *Hastenrath*, 2002] even if the IOD appear as a see-saw mode dramatically in a physical space during event years. The above subtlety is demonstrated mathematically in *Behera et al*. [2003a].

3.3. Ocean–atmosphere Coupling During IOD Events

The dipole mode in the SST anomalies is found to be coupled with subsurface temperature variability as well as atmospheric variability in the Indian Ocean. In fact, the first dominant mode of subsurface temperature variability, in contrast to the second dominant mode of SST variability, is characterized by a dipole related to the IOD [*Rao et al.*, 2002a]. To show a close link between the surface signal and the sub-

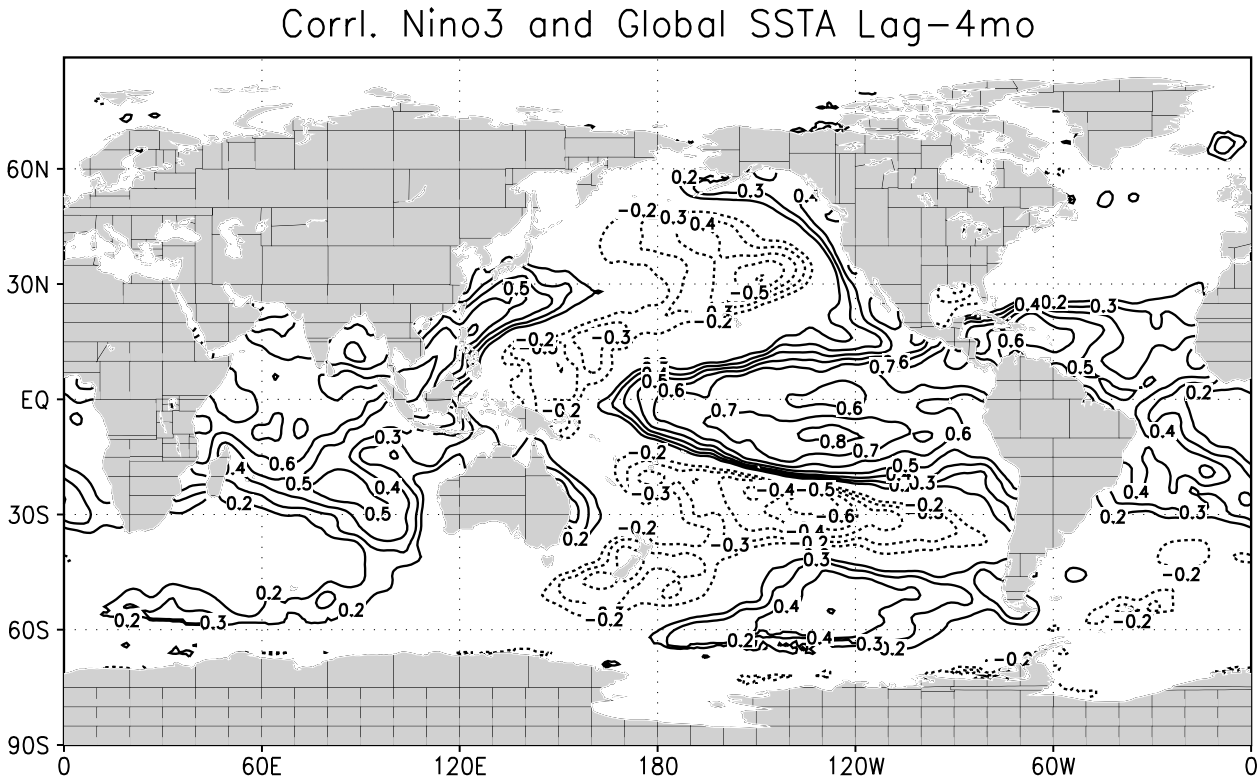

Figure 2. Correlation of the Niño-3 index with the global SST anomalies, when the former is leading the latter by 4 months. Values higher than 99% confidence limit using a 2-tailed t-test are contoured.

surface signal, we calculate an index by taking the area average of the anomalies of upper 125m heat content obtained from SODA. The area used to compute the heat content index is from 60°E–70°E and from 5°S to 5°N. This box falls within the domain of the western pole of the DMI in SST anomalies. Figure 3 shows the correlation between this heat content index and SST and wind stress anomalies during August–November. The high correlation of the heat content index with SST anomalies in the western Indian Ocean along with its simultaneous inverse correlation in the eastern part demonstrates the basin-wide coupling between the surface signal and the subsurface signal during the IOD season. Also, the correlation with equatorial wind anomalies shows the close coupling between the ocean and the atmosphere. Thus the dominant mode of subsurface variability, which is coupled with surface winds, provides a necessary feedback to SST during the IOD events.

The above is confirmed in the region of high correlation between 60°E and 80°E, where a signature of the coupled Rossby waves excited by the IOD-related winds in the equatorial region is prominent [*Rao et al.*, 2002a; *Xie et al.*, 2002]. *Rao et al.* [2002a] found that the evolution of the dominant dipole mode in the subsurface is controlled by equatorial ocean dynamics forced by zonal winds in the equatorial region. The subsurface dipole provides the delayed time required to reverse the phase of the surface dipole in the following year through propagation of oceanic Rossby/Kelvin waves. This is further confirmed from a recent coupled model study [*Gualdi et al.*, 2003]. Thus, the turnabout of the phase of the subsurface dipole leads to the quasi-biennial oscillation (QBO) of the tropical Indian Ocean and may play an important role for the QBO in the Indo–Pacific sector [cf. *Meehl*, 1987].

Rossby waves with interannual periodicity (from 3 to 5 years) are reported in the southern Indian Ocean by *Perigaud and Delecluse* [1993], *Masumoto and Meyers* [1998], *Chambers et al.* [1999] and *White* [2000]. In particular, *Masumoto and Meyers* [1998] concluded that these waves are primarily forced by the wind stress curl along the Rossby wave paths. *Xie et al.* [2002], along this context, have suggested that Rossby waves in the southern Indian Ocean play a very important role in air–sea coupling in the region, claiming also that these Rossby waves are dominantly forced by ENSO. In a more elaborate study, however, *Rao et al.* [2004] have distinguished two regions based on the major difference of forcing. The IOD dominates the forcing of the equatorial Rossby waves in the equatorial waveguide north of 10°S. In higher latitudes, i.e. south of 10^0S, the ENSO influence prevails as discussed by *Xie et al.* [2002] and *Jury and Huang* [2003]. In the following,

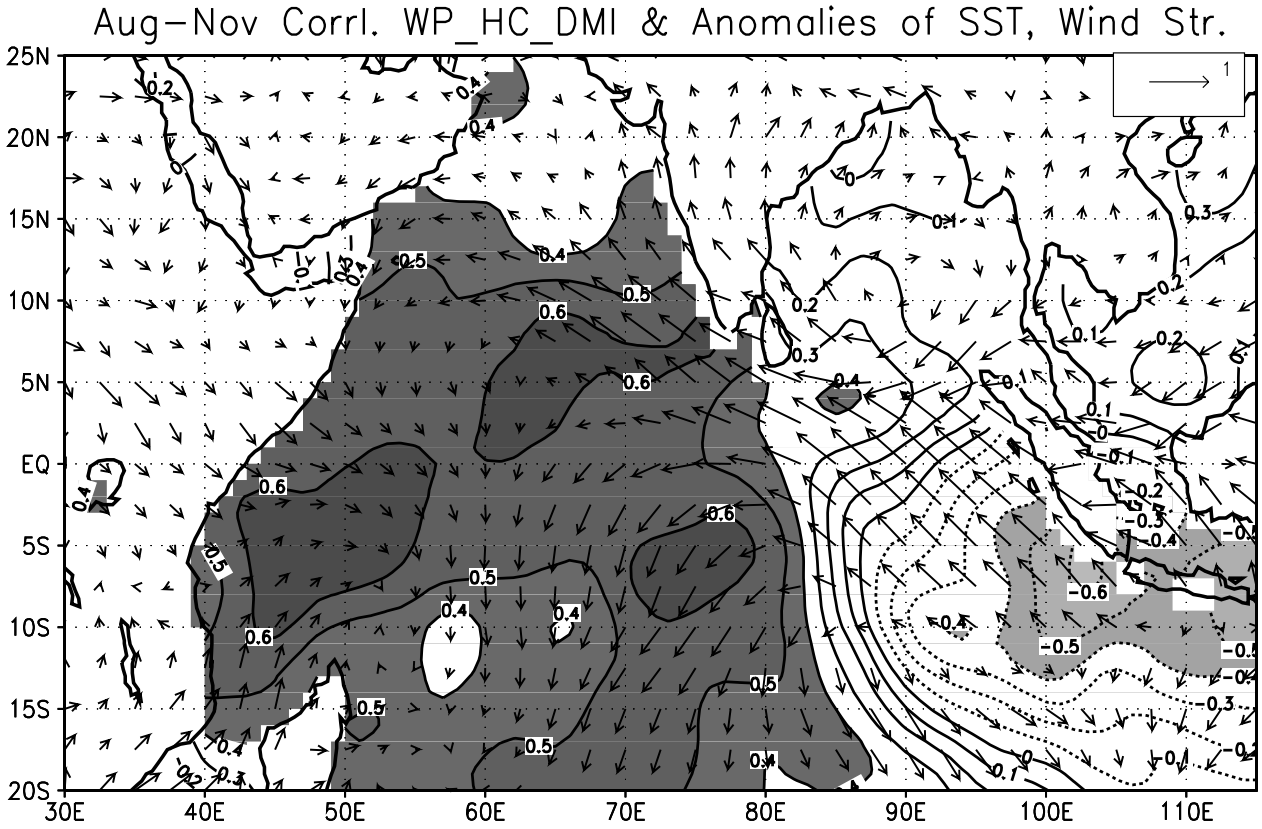

Figure 3. Correlation of the heat content anomaly index from the western box with the SST anomalies from tropical Indian Ocean and the wind stress anomalies. Contour interval is 0.1 and negative (positive) values are indicated by dashed (solid) contours. The contours that exceed ±0.4, which correspond to statistical significance at 99% with a 2-tailed t-test, are shaded.

we further verify this interesting difference in the forcing of Rossby waves using a coupled model simulation.

3.4. Evidence of Coupling in a CGCM Simulation

We here discuss the simulation results from SINTEX-F1 CGCM. Just like the SINTEX [*Gualdi et al.*, 2003], the SINTEX-F1 has shown a very high skill in simulating IOD events as well as ENSO events [*Behera et al.*, 2003b]. Putting aside a comprehensive intercomparison between the SINTEX and SINTEX-F1 simulations, which is beyond the scope of the present paper, we report here some of our analyses that support the observational results. Since the eastern pole of the SST anomaly in the model extends to the central part of the basin, the western box (40°–60°E, 10°S–10°N) used in deriving the model DMI is slightly different from that for the observation (50°–70°E, 10°S–10°N) [*Saji et al.*, 1999]. The standard deviation of the model DMI is 0.5°C that is slightly higher compared to the observed DMI [*Saji et al.*, 1999], whereas the model Niño-3 standard deviation is 0.8°C that is similar to the observation.

As in the observation, we find that the model SST variability is closely coupled to the subsurface variability in the eastern and southern tropical Indian Ocean (Figure 4). We here focus our attention on the air–sea coupling [*Rao et al.*, 2004] in the southern tropical Indian Ocean as it has interesting implications in the African rainfall variability [*Black et al.*, 2003; *Saji and Yamagata*, 2003b; *Behera et al.*, 2003b; *Jury*, 2002]. Seasonal indices of DMI (September–November) and Niño-3 (October–December) are used in the analyses. Figure 5 shows the correlation coefficients between the SSH anomaly at different latitude bands and either the DMI or the Niño-3 index. We note that the correlation in case of the DMI is higher near the equatorial region. In contrast, the correlation with the Niño-3 index is higher in the off-equatorial region. The correlation with the ENSO is not surprising. As discussed in the following section, the analysis is affected by the 28% co-occurrence of IODs with ENSOs. Therefore, we have separated their unique interactions using the partial correlation method here (Figure 6). As evident in Figure 6, the correlation partial to DMI did not change much but the

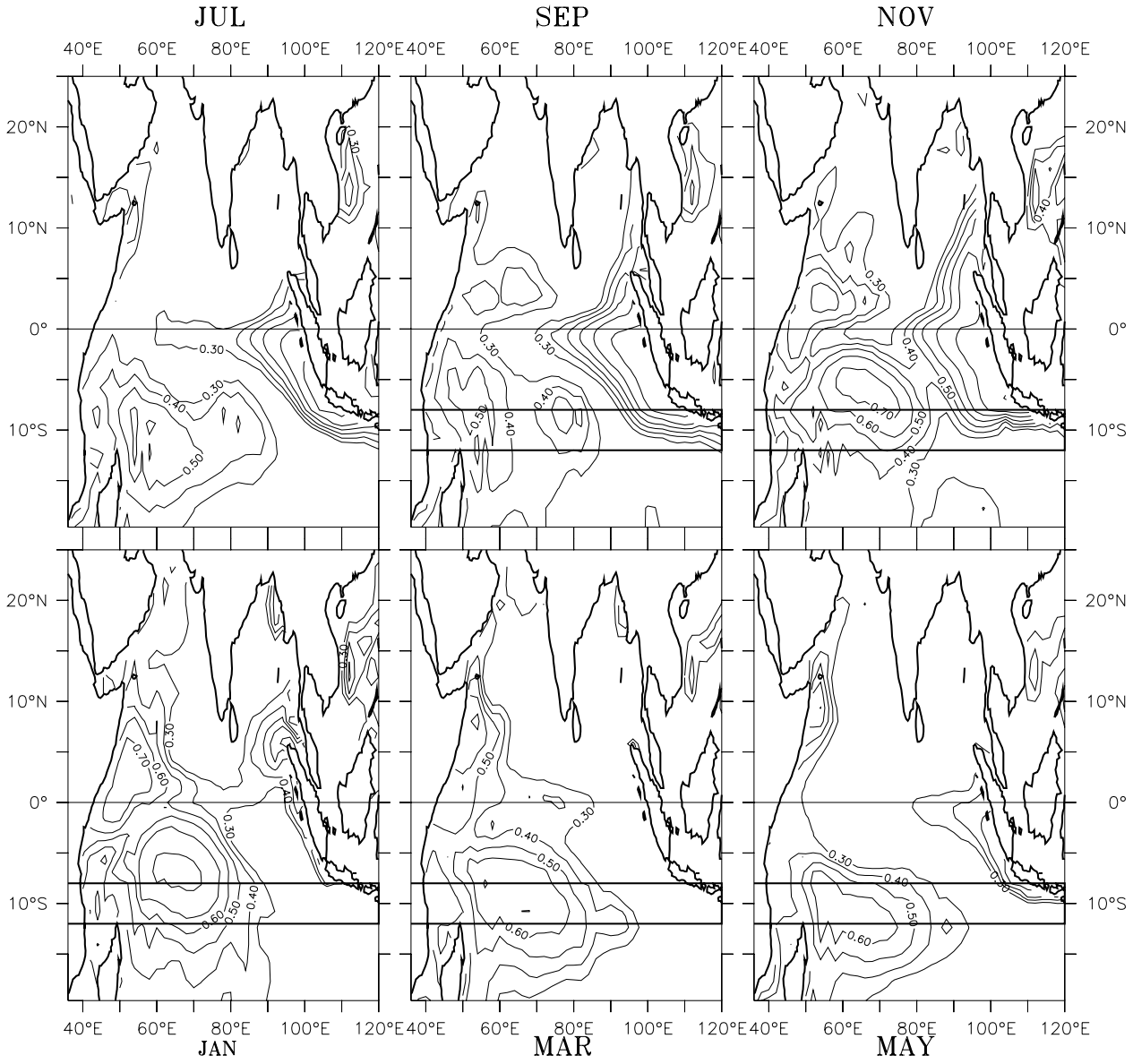

Figure 4. Correlation between the anomalies of SST and SSH from SINTEX-F1 simulation results. Correlations are plotted for alternate months starting from July to the May of the following year. Values higher than 0.2 are statistically significant at 99% level using a 2-tailed t-test.

corresponding correlation partial to Niño-3 weakened appreciably in the equatorial regions. It is interesting to note here that the correlation peaks during boreal fall in the former case, whereas the correlation peaks in spring of the following year in the latter case. Therefore, we must be careful in interpreting relations between the Indian Ocean signals and influences of Pacific climate variations [cf. *Xie et al*., 2002]; the interannual SSH anomalies in the equatorial waveguide north of 10°S is dominated by IOD, whereas that in the off-equatorial region south of 10°S is more influenced by ENSO.

The westward propagation of the long Rossby waves is evident in the correlation patterns; it is particularly clear in the higher latitude bands as the phase speed decreases with the increasing latitude. We note that the theoretical phase speed of the first baroclinic Rossby mode is about 0.7 m s^{-1}, 0.4 m s^{-1}, 0.2 m s^{-1} and 0.1 m s^{-1} for the latitude bands of 2°S–4°S, 6°S–8°S, 10°S–12°S and 14°S–16°S, respectively. Since the phase speed is faster near the equator, the westward orientation is not noticeable in the correlation pattern. We also note that the actual phase propagation can differ from that of the free

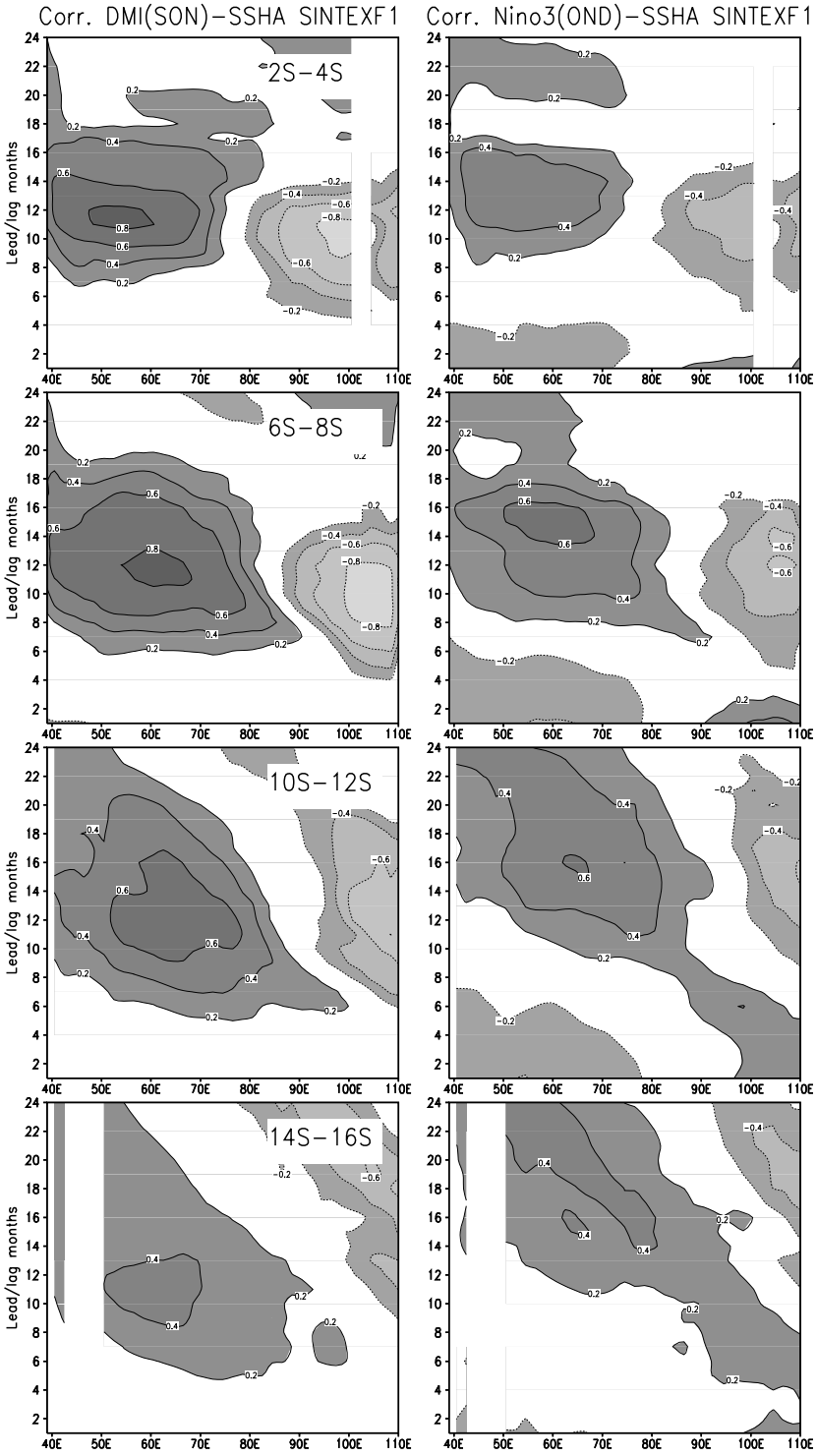

Figure 5. Correlation between the September–November DMI and the south Indian Ocean SSH anomalies (left panels) for different latitude bands in SINTEX-F1 simulation. The corresponding correlation for the October–December Niño-3 index is shown on the right panels. Contour interval is 0.2 and negative (positive) values are indicated by dashed (solid) contours. The contours that exceed ±0.2, which correspond to statistical significance at 99% with a 2-tailed t-test, are shaded.

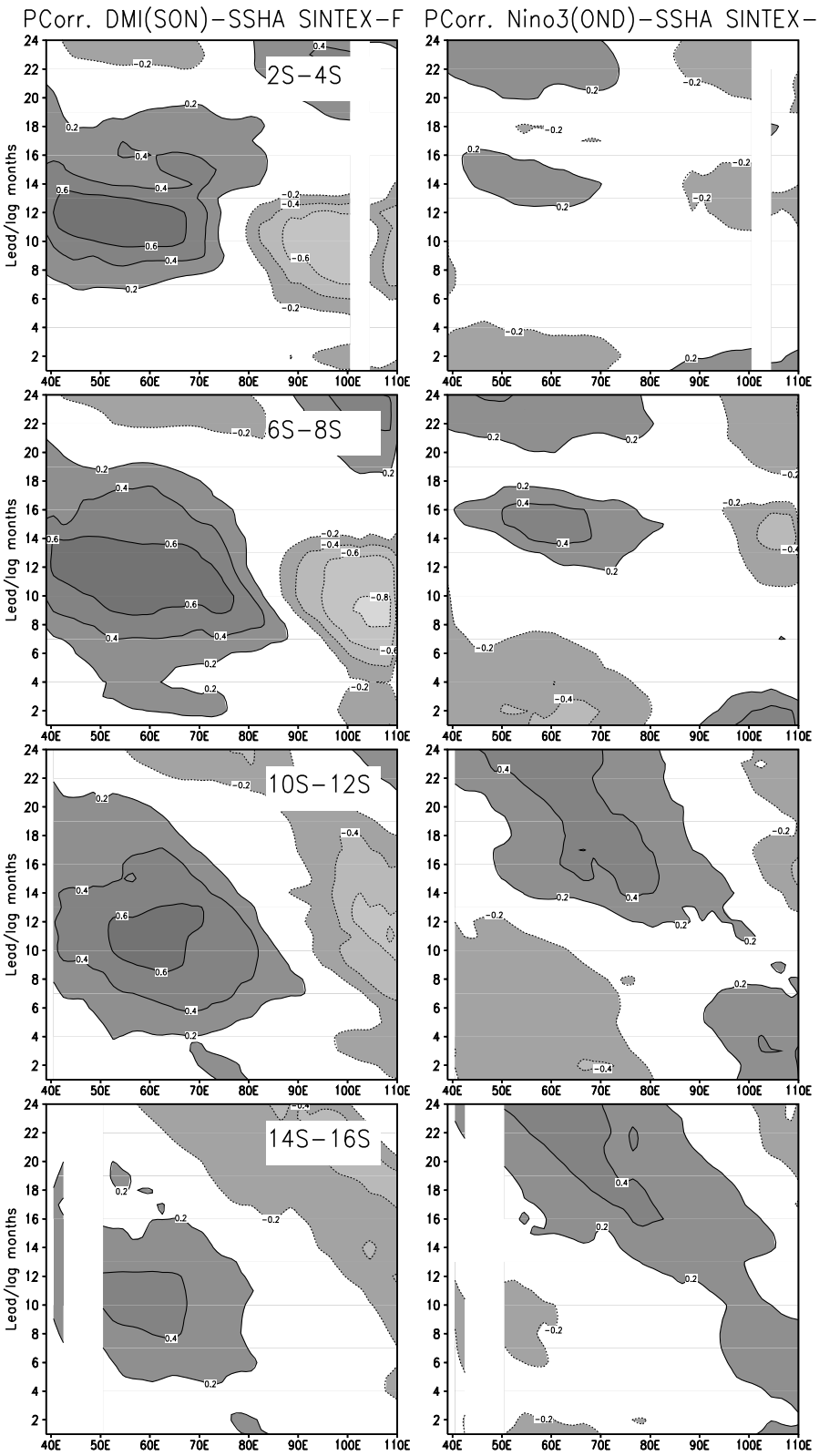

Figure 6. Same as Figure 5 but for the partial correlation.

modes since the waves in the southern Indian Ocean are much influenced by air–sea coupling [e.g., *White,* 2000]. All those from the model simulation are in good agreement with the observations [*Rao et al.*, 2004].

In order to understand the unique nature of subsurface coupling with winds in the model, we have calculated the partial correlation between the wind stress curl anomaly and either the DMI or the Niño-3 index (Figure 7). The correlation partial to DMI becomes significant from July. In particular, high values of correlation are observed in south-central tropical Indian Ocean region during the peak IOD season of September–November. The correlation partial to Niño-3 is insignificant during this time. It becomes significant only in December in a small region south of 10°S. Therefore, it is clear that the ocean–atmosphere conditions related to the IOD is essential for the coupled Rossby waves in the southern equatorial regions. The wind stress curl associated with the IOD forces the westward propagating downwelling long Rossby waves which increase the heat content of the upper layer in the central and western parts of the basin. The heat content anomaly maintains the SST anomaly, which is, in turn, tied to the wind stress anomalies, thereby completing the feedback loop. The ENSO correlation with the southern Indian Ocean is not very clear. One possibility is the ENSO signal through the Indonesian throughflow. The oceanic anomaly of the Pacific origin may propagate westward and enhance local air–sea coupling south of 10°S, thus generating wind anomalies necessary to excite the Rossby waves in the higher latitude [cf. *Masumoto and Meyers*, 1998].

4. IOD AS AN INHERENT COUPLED MODE

As already mentioned, the IOD events sometimes co-occur with the Pacific ENSO events in both the present model and the observation. Therefore, one concern about IOD is whether it is independent from ENSO. A simple correlation between DMI and Niño-3 index is 0.33 in the observation [*Saji et al*., 1999]. Since the IOD evolution is locked to seasons, it is important to introduce the seasonal stratification in the statistical analysis as pointed out by *Nicholls and Drosdowsky* [2000] and *Allan et al*. [2001]. For the peak IOD season of September–November, the correlation between DMI and Niño-3 index amounts to 0.53. Based on this significant correlation, one is apt to conclude in a straightforward way that IOD events occur as a part of ENSO [*Allan et al.*, 2001; *Baquero-Bernal et al*., 2002]. Another way in interpreting this statistics is that it merely reflects the fact that one third of the positive IOD events co-occur with El Niño events. The latter view is based on the fact that the non-orthogonality of two time series does not necessarily mean that the two phenomena are always connected in a physical space. Observation of clear independent occurrence of IOD in some years as discussed in the following tilts the discussion in favor of the latter interpretation.

Several positive IOD events actually evolved in absence of El Niño in certain years such as 1961, 1967 and 1994. This is further analyzed using a composite technique. In addition to composite pictures based on all IOD and ENSO events, we have prepared composites for pure events. A positive (negative) pure IOD event is identified as an event when El Niño (La Niña) does not co-occur (Table 1). In total, 9 independent IOD events and 10 independent ENSO events are used to prepare composite pictures for pure events. The total number assures us of robustness of the results. Figure 8 shows such composites of SST anomalies for all and pure IOD events during the IOD evolution period. Both composites look very similar. We find cold SST anomalies near the Sumatra coast and in the eastern Indian Ocean and warm SST anomalies in the regions of central and western Indian Ocean. It may be noted that the SST anomalies are stronger in the pure IOD composite. To understand the characteristics of the ENSO-related anomalies during those months, we have plotted in Figure 9 the corresponding composites of SST anomalies. Although a dipole-like pattern emerges in all El Niño composite, it almost disappears in a pure El Niño composite (right panel in Figure 9) in which we have removed the co-occurring IOD years. In the pure El Niño composite, we find that the cold SST anomalies near the Java coast propagate along the west coast of Australia. This is understood on the basis of the oceanic finding that the mature ENSO signal in the western Pacific intrudes into the eastern Indian Ocean through the coastal wave-guide around the Australian continent [*Clarke and Liu*, 1994; *Meyers*, 1996]. The SST in the eastern Indian Ocean near the west coast of Australia during the boreal fall and winter is thus influenced by ENSO. This is known as the *Clarke-Meyers effec*t. The changes in the SST may cause local air–sea interaction in this region [*Hendon*, 2003; *Tozuka and Yamagata*, 2003]. This phenomenon appears to be different from the cooling off Sumatra related to the basin-wide IOD phenomenon that involves the equatorial ocean dynamics as discussed earlier. However, it apparently enhances the IOD-ENSO correlation during the boreal fall.

As discussed earlier, the variability of the IOD and ENSO is simulated realistically in the SINTEX-F1 CGCM. The correlation between DMI and Niño-3 is 0.4 for the whole year and 0.54 for the boreal fall season, which is very similar to the observation. Therefore, the long time series of the model simulation gives us an opportunity to verify the above independence issue of IOD with better statistical confidence. We have shown the composite of anomalies of model SST and SSH in Figures 10 and 11. Here we only show the composites for pure IOD and pure ENSO events. In total, we find 25 pure IOD events and 15 pure ENSO events in the model simulation.

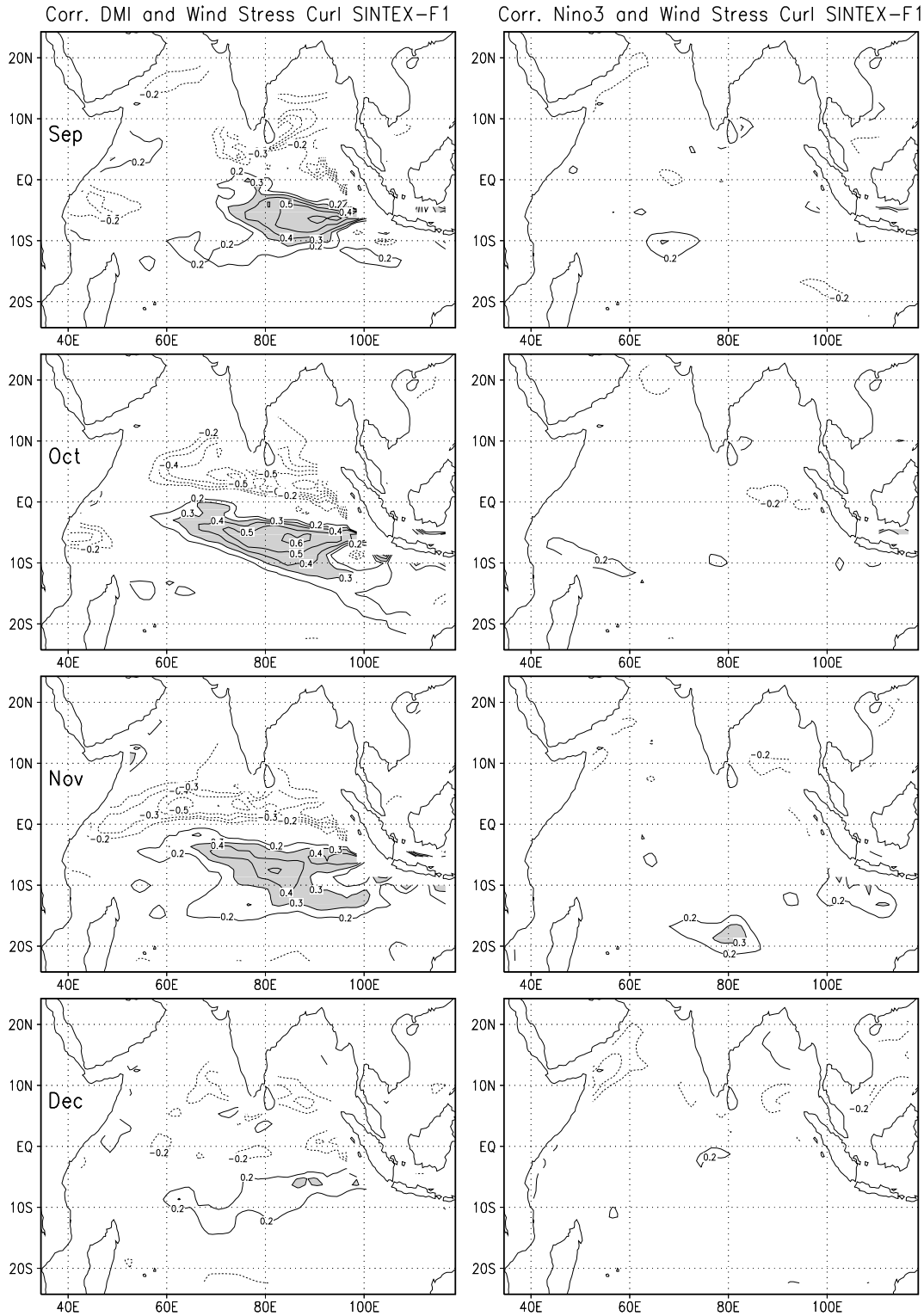

Figure 7. Same as Figure 5 but for the partial correlations with the tropical Indian Ocean wind stress curl anomalies for the months starting from September to December. Contoured values are statistically significant at 99% level using a 2-tailed t-test and positive values > 0.3 are shaded.

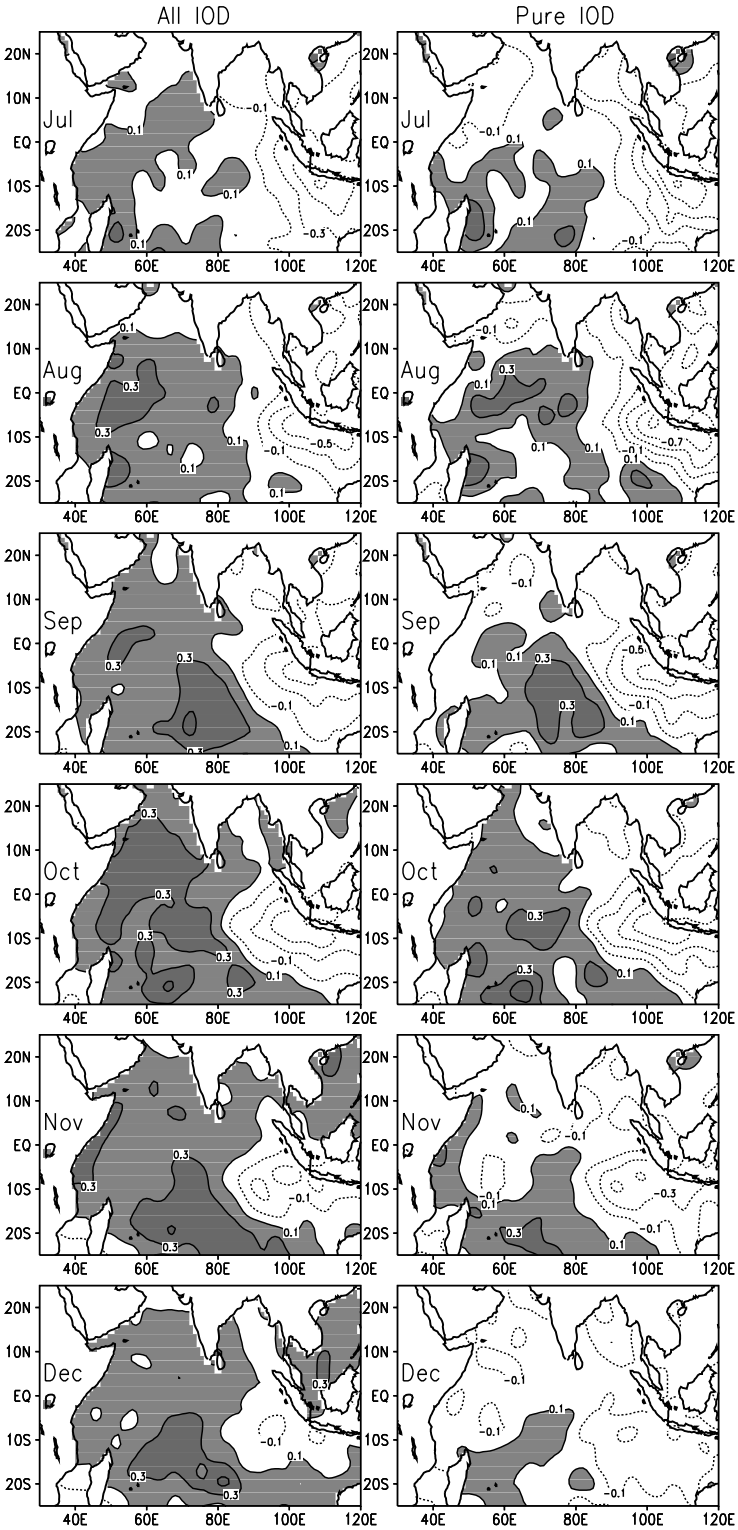

Figure 8. Composite ((positive–negative)/2) plots of SST anomalies for months starting from July to December. Left panels show the composite for the IOD years that also include ENSO events. Right panels are the composites for the pure IOD years. Contour interval in 0.2^0C and positive values > 0.1^0C are shaded.

Table 1. Years of IOD and ENSO events considered in the composite analyses. The asterisk denotes pure events, i.e. no El Niño (La Niña) during a positive (negative) IOD event.

	Years of Positive IOD	Years of Negative IOD	Years of El Niño	Years of La Niña
1	**1961***	**1958***	1963	1964
2	1963	**1960***	**1965***	**1967***
3	**1967***	1964	**1969***	1970
4	1972	1970	1972	**1971***
5	**1977***	**1989***	**1976***	**1973***
6	1982	**1992***	1982	**1975***
7	**1994***	**1996***	**1986***	**1988***
8	1997	-	**1991***	-
9	-	-	1997	-

The evolution of IOD events is clearly seen in the pure IOD composites but the dipole-like variability cannot be seen in the pure ENSO composites. Rather, we notice the basin-wide uniform mode. These model results, together with the observed data, demonstrate the existence of the independent evolution of IOD.

The zonal Walker circulation is another process that may link the IOD events in the Indian Ocean with ENSO events in the Pacific. *Yamagata et al*. [2002] have shown that the atmospheric bridge between the two basins is apparent when we consider all IOD events that include the co-occurring ENSO events. However, they have demonstrated that an anomalous Walker cell exists only in the Indian Ocean during pure IOD events [Figure 4 of *Yamagata et al*., 2003]; this also confirms the independent evolution of some IOD events. To avoid misunderstanding, we repeat that this linear analysis does not exclude completely the possibility of physical interaction between the two climate signals in some cases. From a case study of the 1997–98 El Niño event, *Ueda and Matsumoto* [2000] suggested that the changes in the Walker circulation related to the El Niño could influence the evolution of IOD through changes in the monsoon circulation. Conversely, *Behera and Yamagata* [2003] showed that IOD modulates the Darwin pressure variability, i.e., the Southern Oscillation.

The precondition for IOD evolution is yet another issue for deliberation. Several studies indicate presence of a favorable mechanism in the eastern Indian Ocean [e.g., *Saji et al*., 1999; *Behera et al*., 1999] that combines cold SST anomalies, strengthening of southeasterlies and suppression of convection into a feedback loop. However, recent studies offer a few alternatives: atmospheric pressure variability in the eastern Indian Ocean [e.g., *Gualdi et al*., 2003; *Li et al*., 2003], favorable changes in winds in relation to the Pacific ENSO and Indian monsoon [e.g., *Annamalai et al*., 2003] and influences from the southern extratropical region [e.g., *Lau and Nath*, 2004]. All those studies fall short in more than one occasion to answer the failure (success) in IOD evolution in spite of favorable (unfavorable) precondition. For example, *Gualdi et al*. [2003] reported the failure of their proposed favorable mechanism to excite the IOD event in 1979. We also find several instances (e.g. the aborted 2003 event) when an IOD event is aborted at its premature stage although air–sea conditions are apparently favorable for its complete evolution. This indicates the evolution mechanism of the IOD is more complex than we expect now and we need further studies. Processes that need immediate attention are 1) mechanisms that connect/disconnect subsurface signals with surface ones including the barrier layer structure [*Masson et al*., 2003a], and 2) roles of intraseasonal disturbances in both atmosphere and ocean. The IOD's unique influence on the global climate as reviewed in the following section provides motivation for further intensive field and modeling efforts.

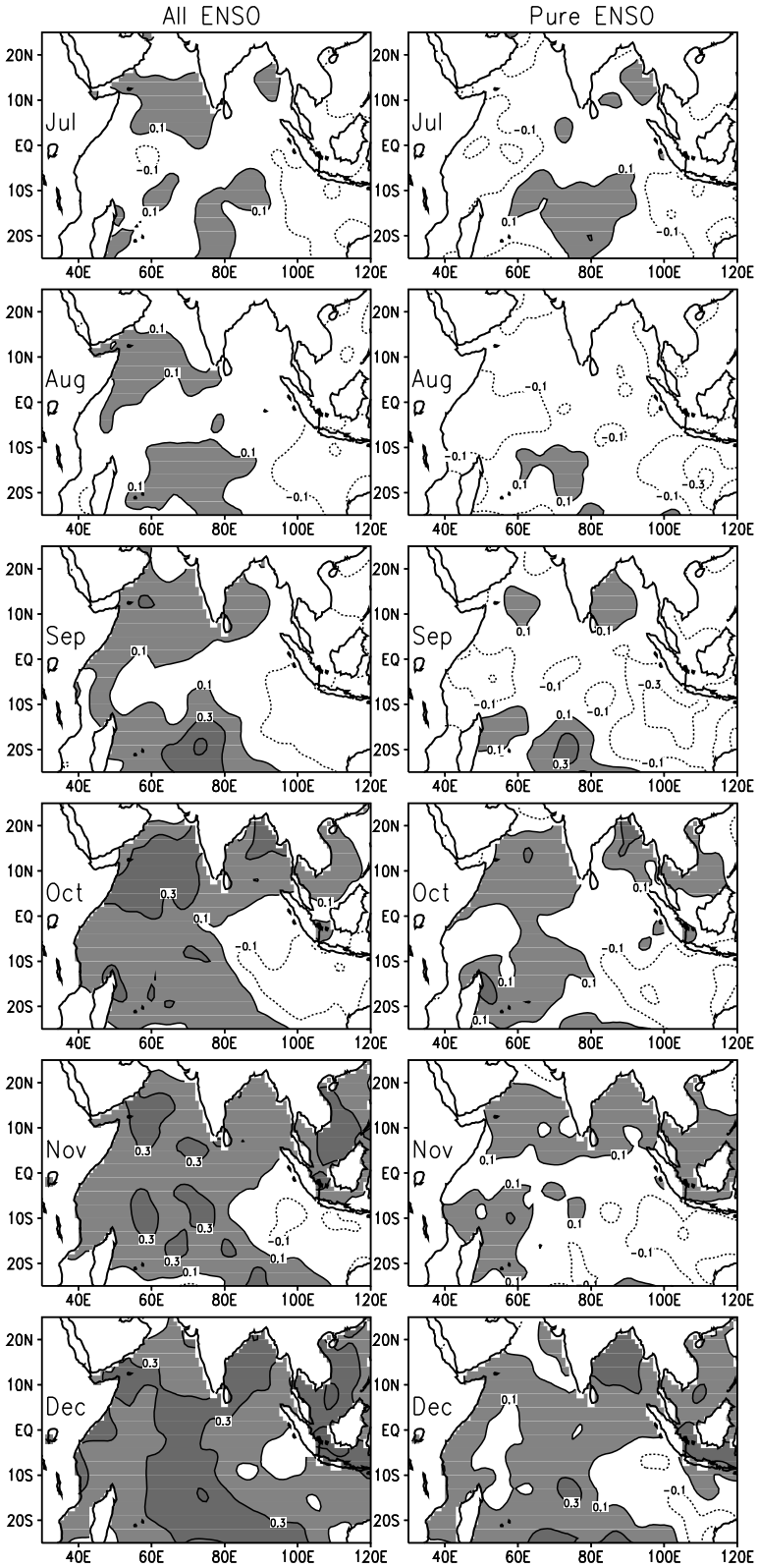

Figure 9. Same as Figure 8 but for all and pure ENSO years.

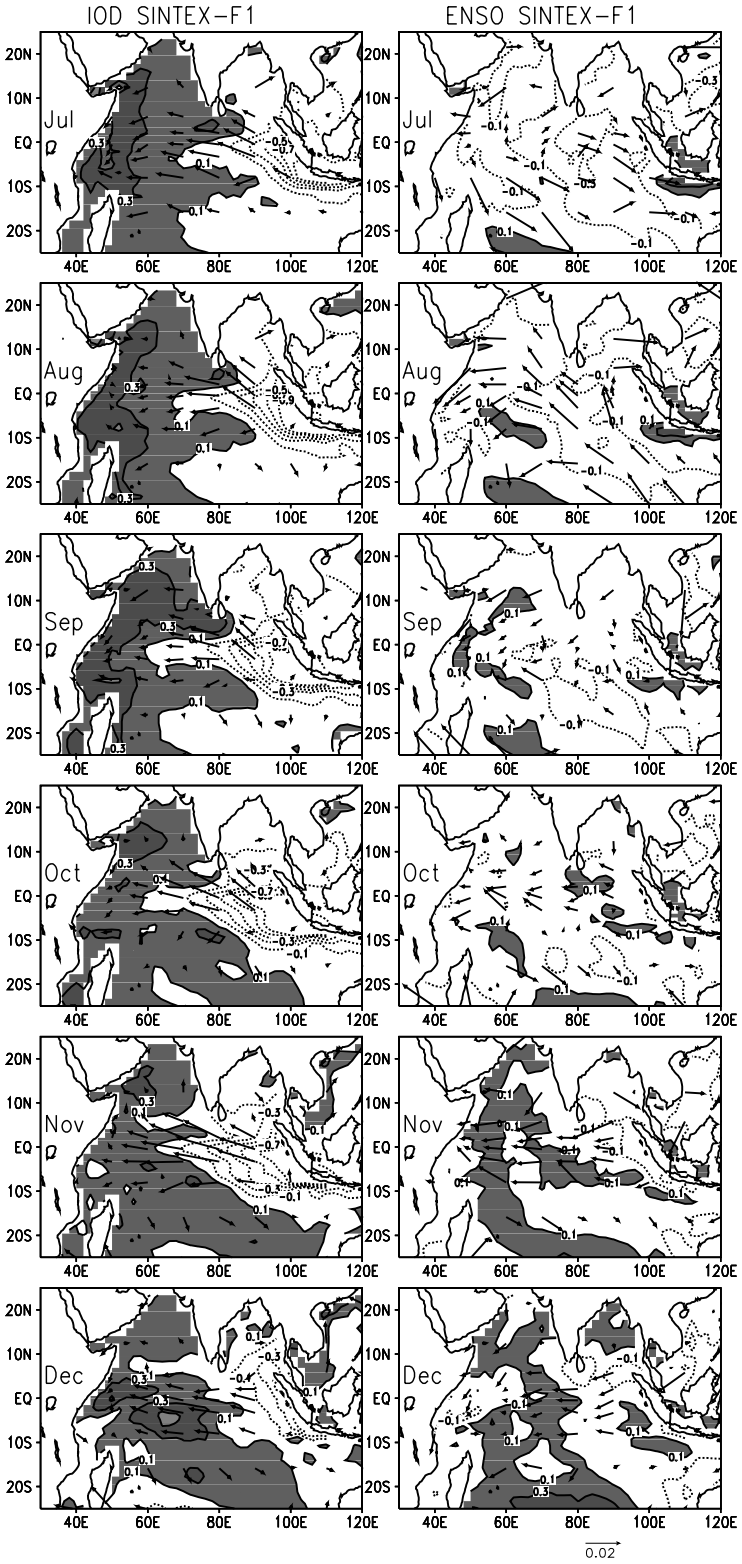

Figure 10. Same as Figure 8 but for the composites of SST (^{0}C) and wind stress (Nm^{-2}) anomalies from SINTEX-F1 simulation results for pure IOD events (left panels) and pure ENSO events (right panels).

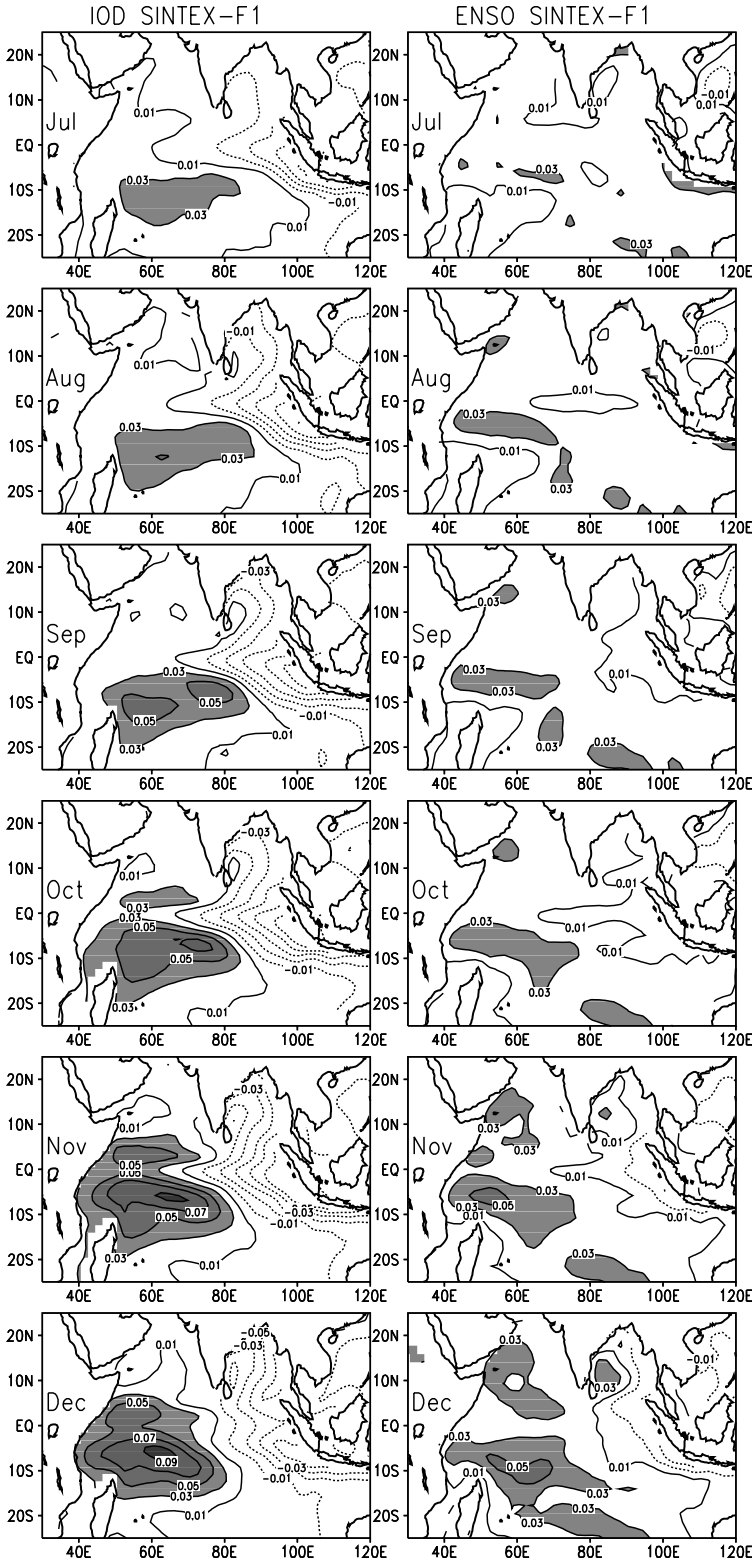

Figure 11. Same as Figure 10 but for model SSH anomalies. Contour interval is 0.02 m and positive values > 0.03 m are shaded.

5. IOD TELECONNECTION

One of the most important directions of the IOD research from the societal viewpoint is the identification of its unique teleconnection bringing regional climate variability in various parts of the globe. Since IOD and ENSO indices are not completely orthogonal, IOD influences must be carefully appreciated. Now that the degeneracy is almost resolved using the partial correlation analysis, relative influences caused by these two major tropical phenomena are becoming clear. *Behera and Yamagata* [2003] showed that the IOD influences the Darwin pressure variability, i.e., Southern Oscillation. Positive IOD and El Niño have similar impacts in the Indonesian region owing to anomalous atmospheric subsidence, and thereby induce drought there. Interested readers are referred to *Saji and Yamagata* [2003b], where they have shown for the first time, using the partial correlation analysis, the IOD teleconnection pattern over the globe.

Here, we show rainfall variabilities associated with either IOD or ENSO using a composite technique which is similar to but much simpler than the partial correlation analysis. Plate 1 shows the composite plots for two consecutive seasons. Notice that the anomalies in the East African region are unlike those from a conventional view. Several previous studies suggested enhanced short rains during El Niño events [*Ropelewski and Halpert*, 1987; *Ogallo*, 1989; *Hastenrath et al*., 1993; *Mutai and Ward*, 2000]. Recent statistical analyses of observed data, however, have revealed that IOD rather than El Niño is more responsible for the enhancement of the East African short rains [*Black et al.*, 2003; *Saji and Yamagata,* 2003b]. Plate 1 supports clearly this new view. In addition, *Behera et al*. [2003b], after deriving an index for the East African short rains, have shown that SINTEX-F1 simulation results reproduces an east–west dipole in the correlation between the short rain index and the SST anomalies in the Indian Ocean. They have also found a high simultaneous correlation of the zonal wind anomalies, emphasizing the existence of air–sea coupling during the IOD's influence on the East African short rains. The slow propagation of the air–sea coupled mode in the western Indian Ocean provides a scope for the predictability of the IOD-induced short rains at least a season ahead [*Rao et al*., 2004]. The anomalous westward low-level winds in response to the anomalous zonal gradient of SST increase the moisture transport to the western Indian Ocean and enhance atmospheric convection in East Africa. The model DMI has a high correlation coefficient of 0.65 with that for East African short rains. In contrast, the model Niño-3 index has a correlation coefficient of only 0.28 with that for East African short rains. In Plate 2, we show the partial correlation of the model rainfall anomalies with either DMI or Niño-3. The correlation patterns are consistent with the observed variation of rainfall anomalies in the East African region; positive IOD (El Niño) events are related to enhanced (reduced) rainfall in East Africa. Interestingly, the current coupled model captures even the higher impact of IOD on the Sri Lankan Maha rainfall as observed by *Lareef et al*. [2003]. In the Indonesian regions, the model rain anomaly shows higher negative partial correlation with the IOD index as compared to that of ENSO.

From the rainfall composite plots in Plate 1 and similar composites for surface temperature (figures not shown), we find that the positive IOD and El Niño have opposite influences in the Far East, including Japan and Korea; positive IOD events give rise to warm and dry summer, while negative IOD events lead to cold and wet summer [see *Saji and Yamagata*, 2003b for more details]. For example, the record-breaking hot and dry summer during 1994 (just like 1961) in East Asia was actually linked to the IOD [*Guan and Yamagata*, 2003]. It is well known that the summer climate condition over East Asia is dominated by activities of the East Asian summer monsoon system. Since the East Asian summer monsoon system is one subsystem of the Asian Monsoon [*Wang and Fan*, 1999], it interacts with another subsystem, the Indian summer monsoon, via variations of the Tibetan high and the Asian jet [*Rodwell and Hoskins*, 1996; *Enomoto et al*., 2003]. The precipitation over the northern part of India, the Bay of Bengal, Indochina and the southern part of China was enhanced during the 1994 positive IOD event [*Behera et al*., 1999; *Guan and Yamagata*, 2003; *Saji and Yamagata*, 2003b]. Using the NCEP/NCAR reanalysis data [*Kalnay et al.*, 1996] from 1979 through 2001 and the CMAP precipitation data from 1979 through 1999, *Guan and Yamagata* [2003] analyzed the summer conditions of 1994 and found that the equivalent barotropic high pressure system known as the Bonin High was strengthened over East Asia (Figure 12). The anomalous pressure pattern bringing the hot summer is well known to Japanese weather forecasters as a whale tail pressure pattern. The tail part (the Bonin High) is equivalent barotropic in contrast to the larger baroclinic head part the Pacific High). The IOD-induced summer circulation changes over East Asia are understood through a triangular mechanism as shown schematically in Plate 3. One process is that a Rossby wavetrain is excited in the upper troposphere by the IOD-induced divergent flow over the Tibetan Plateau [*Sardeshmukh and Hoskins*, 1988]. This wave train propagates northeastward from the southern part of China. This is quite similar to Nitta's Pacific–Japan pattern [*Nitta*, 1987] although the whole system is shifted a little westward. Another process is that the IOD-induced diabatic heating around India excites a long atmospheric Rossby wave to the west of the heating. The latter reminds us of the monsoon–desert mechanism that connects the circulation changes over the Mediterranean Sea/Sahara region with the heating over India [*Rodwell and Hoskins*, 1996]. Interestingly, this monsoon–desert mecha-

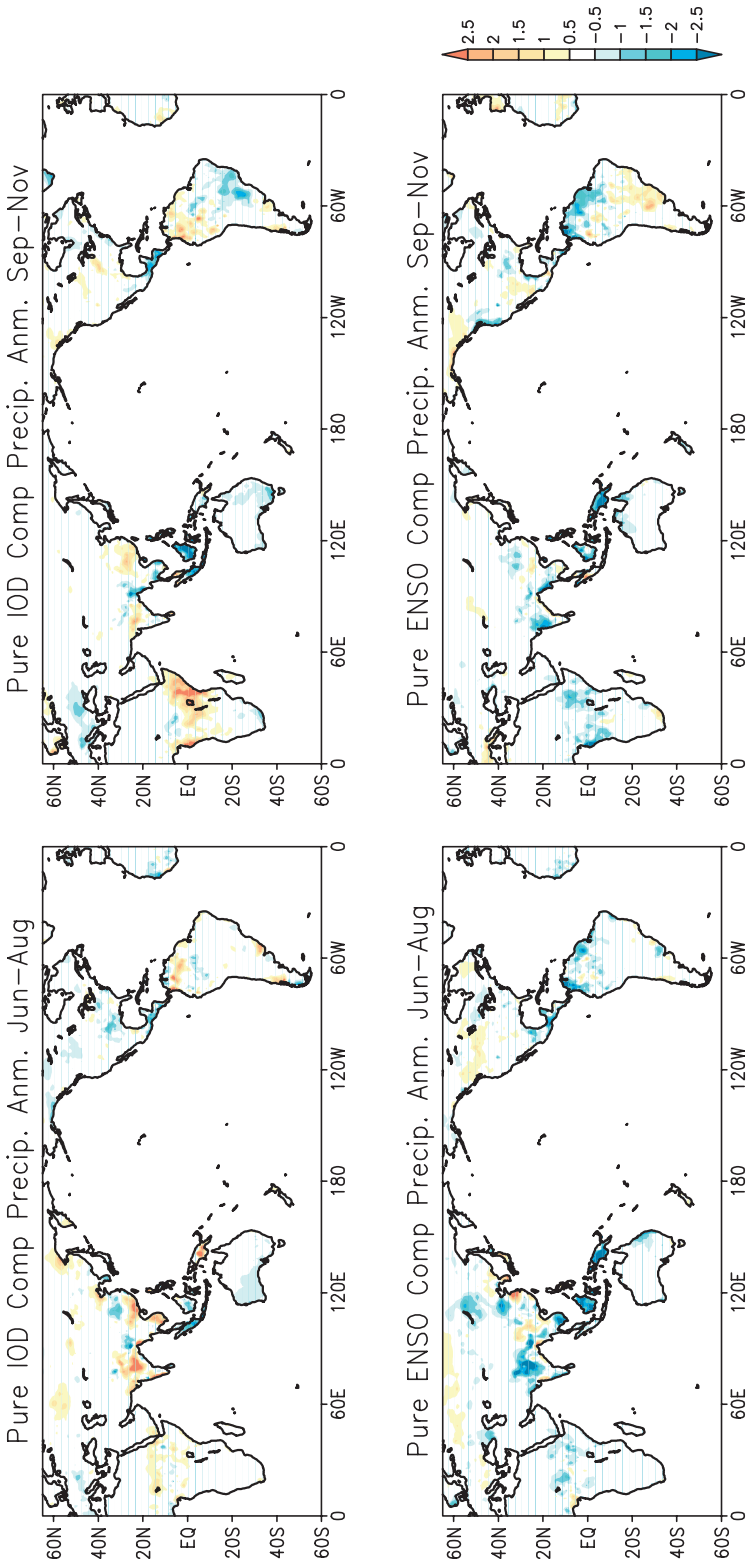

Plate 1. Composites of gridded precipitation anomalies (mm/day) for pure IOD (upper) and ENSO (lower) events. The left panels are for June–August season and the right panels are for September–November season.

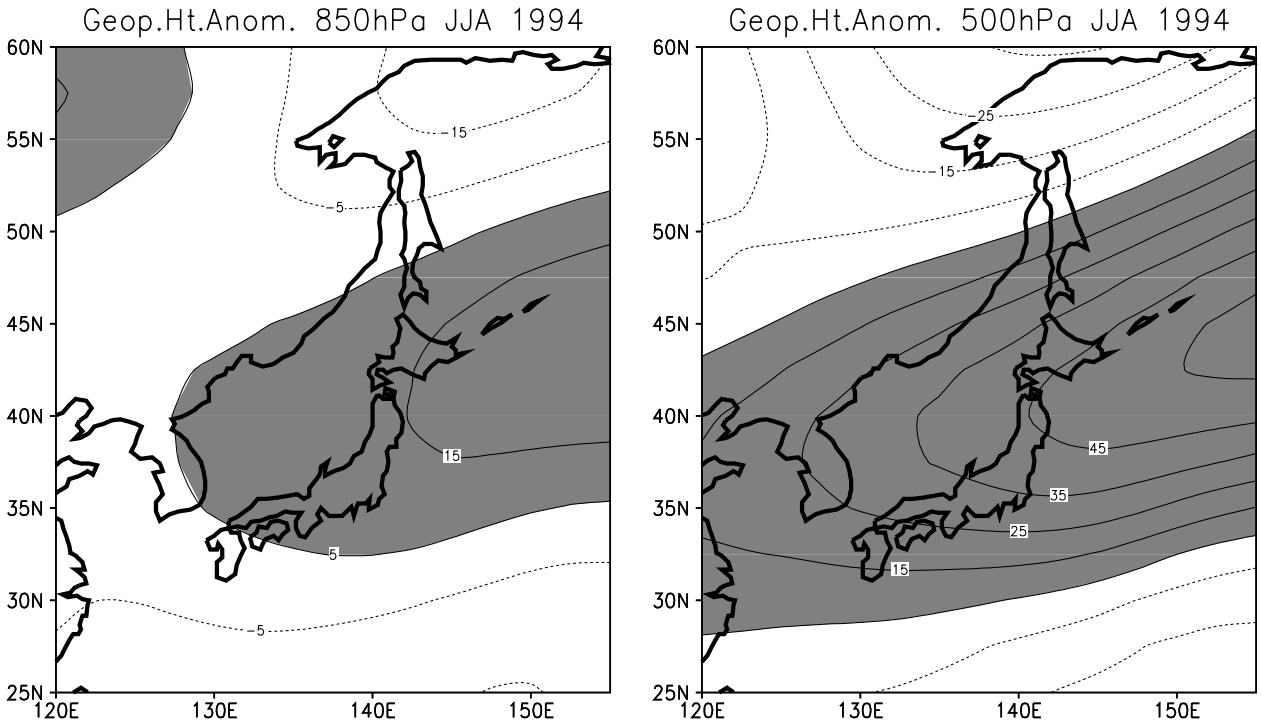

Figure 12. June–August geopotential height anomalies during summer of 1994 for 850 hPa (left) and 500 hPa (right).

nism was introduced by examining the anomalous summer condition of 1994 prior to the discovery of IOD [cf. *Hoskins*, 1996]. The westerly Asian jet acts as a waveguide for eastward propagating tropospheric disturbances to connect the circulation change around the Mediterranean Sea with the anomalous circulation changes over East Asia. This mechanism called the Silk Road process may contribute to strengthening the equivalent barotropic Bonin High in East Asia [*Enomoto et al*., 2003]. The scenario was confirmed by calculating the wave activity flux [cf. *Plumb*, 1986; *Takaya and Nakamura*, 2001] by *Guan and Yamagata* [2003].

In the Southern Hemisphere, the impact of the IOD is remarkable in the southwestern part of Australia [*Saji et al*., 2003b; *Ashok et al*., 2003b] and Brazil [*Saji et al*., 2003b]; positive IOD events cause warm and dry conditions and negative events cause cold and wet conditions (Plates 1 and 2). The IOD teleconnection in the winter hemisphere is more like a Rossby wave train.

6. SUMMARY

Using various ocean and atmosphere data, we have shown that the IOD is a natural ocean–atmosphere coupled mode in the Indian Ocean. This important tropical ocean–atmosphere coupled phenomenon has been overlooked for a long period as the ENSO-forced basin-wide mode dominates statistically the SST variability in the basin. The SINTEX-F1 CGCM simulates successfully the IOD as an ocean–atmosphere coupled mode and confirms the importance of oceanic dynamics in the evolution of IOD.

Although the IOD emerges statistically as the second major mode in observed SST anomalies, it shows up as a remarkable event in some years, just like a normal mode in classical dynamics, and induces climate variations in many parts of the world. The year of 1994 was such a case and the dramatic impact on summer conditions in East Asia actually led the authors to shed light on this important climate signal as a synthesis of the phenomenon described in part in the past. We have discussed here how the IOD event influences summer conditions in East Asia mostly on the basis of our recent work. The abnormally hot and dry summer in 1994 was induced by the IOD-related rainfall anomalies in South Asia through a triangular mechanism (Plate 3). On the eastern side of the triangle, the mechanism is similar to the Nitta's Pacific–Japan pattern with slight westward shift. The combination of monsoon–desert mechanism and the Silk Road process on the other two sides of the triangle strengthens the Bonin High over Japan as a whale tail pattern.

The air–sea coupling in the western Indian Ocean related to the IOD events produces anomalously active short rains in East Africa. During a positive event the wind stress curl anomalies in the off-equatorial region of the central part, related

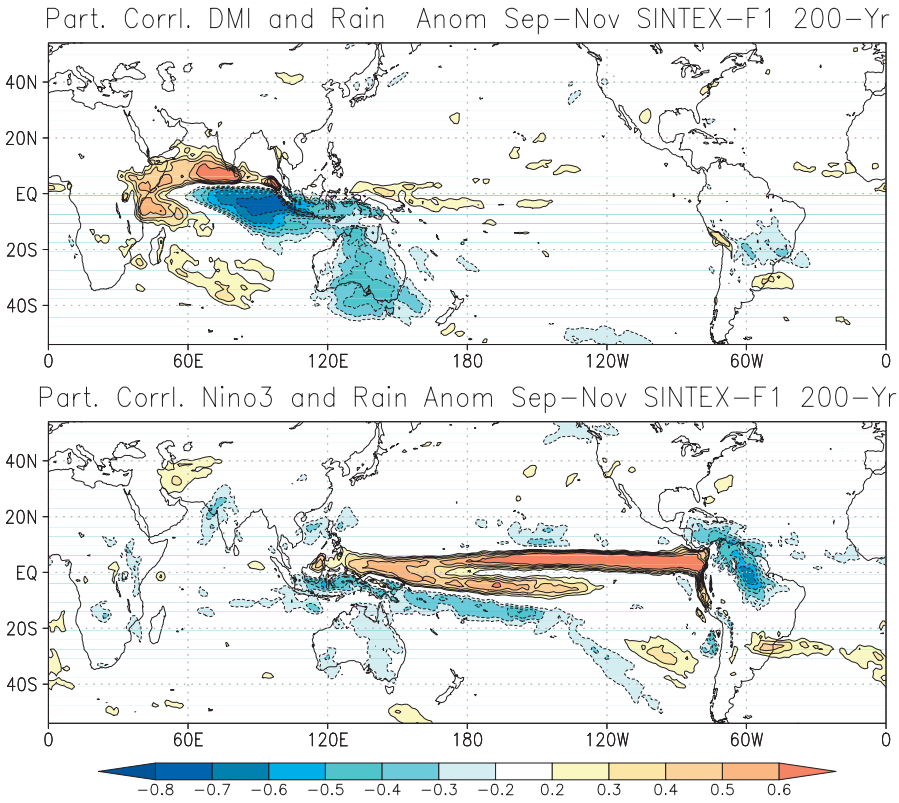

Plate 2. Partial correlation of model DMI with rainfall anomalies. The upper panel shows the partial correlation of the model DMI with the rainfall anomalies (where the Niño-3 influence is removed from the correlation) and the lower panel shows the corresponding partial correlation for the Niño-3 index (where the DMI influence is removed from the correlation). Shaded values are statistically significant at 99% level using a 2-tailed t-test.

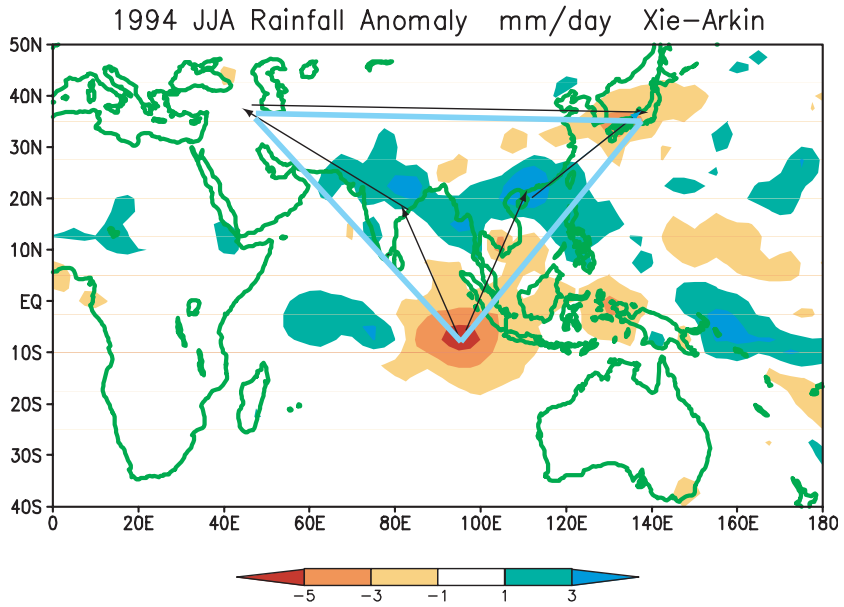

Plate 3. Schematic of the 1994 IOD event influence on the East Asia summer conditions. The triangular mechanism is shown over the shaded rainfall anomalies.

to the changes in the atmospheric convection near Sumatra, produces warmer SST. This, together with the zonal gradient in the SST anomalies in the tropical region, enhances moisture transport to the East Africa and thereby induces higher rainfall there. This is verified here by the CGCM simulation. The influence of the IOD is also remarkable in the Southern Hemisphere, particularly over Australia and Brazil. Interestingly, this observed behavior (Plate 1) is also well simulated by the SINTEX-F1 CGCM (Plate 2).

Understanding the teleconnection patterns related to either IOD or ENSO and their positive/negative interference during years of co-occurrence is very important from a societal viewpoint because people at large suffer from their regional influences rather than the coupled phenomena themselves. We have shown here that the SINTEX-F1 model simulates such climate signals and their influences reasonably well. Predicting the regional derivatives of climate variations is becoming a challenge [cf. *Philander*, 2004]. Despite the complexity in the coupled system, recent progress in high-resolution CGCM development along with the increased interest in setting up the Indian Ocean observing network composed of TRITON buys, ARGO floats and proposed equatorial moorings will enhance our understanding and predictability of the coupled variability in the Indian Ocean.

Acknowledgments. Discussions with Drs. Ashok, Delecluse, Gualdi, Guan, Meyers, Navarra, Philander, and Saji were very helpful in preparing this review from our new viewpoint. Two anonymous reviewers provided useful suggestions.

REFERENCES

Abram, N. J., M. K. Gagan, M. T. McCulloch, J. Chappell, and W. S. Hantoro, Coral reef death during the 1997 Indian Ocean Dipole linked to Indonesian wildfires, *Science, 301*, 952–955, 2003.

Allan, R., D. Chambers, W. Drosdowsky, H. Hendon, M. Latif, N. Nicholls, I. Smith, R. Stone, and Y. Tourre, Is there an Indian Ocean dipole, and is it independent of the El Niño–Southern Oscillation? *CLIVAR Exchanges*, *6*, 18–22, 2001.

Annamalai, H., R. Murtugudde, J. Potemra, S. P. Xie, P. Liu, and B. Wang, Coupled dynamics over the Indian Ocean: Spring initiation of the zonal mode, *Deep-Sea Res. II*, *50*, 2305–2330, 2003.

Ashok, K., Z. Guan, and T. Yamagata, Impact of the Indian Ocean Dipole on the Decadal relationship between the Indian monsoon rainfall and ENSO, *Geophys. Res. Lett*., *28*, 4499–4502, 2001.

Ashok, K., Z. Guan., and T. Yamagata, A look at the relationship between the ENSO and the Indian Ocean Dipole, *J. Meteorol. Soc. Jpn.*, *81*, 41–56, 2003a.

Ashok, K., Z. Guan, and T. Yamagata, Influence of the Indian Ocean Dipole on the Australian winter rainfall, *Geophys. Res. Lett*., *30,* doi:10.1029/2003GL017926, 2003b.

Baquero-Bernal, A., M. Latif, and S. Legutke, On dipole-like variability in the tropical Indian Ocean, *J. Clim., 15*, 1358–1368, 2002.

Behera, S. K., R. Krishnan, and T. Yamagata, Unusual ocean–atmosphere conditions in the tropical Indian Ocean during 1994, *Geophys. Res. Lett., 26*, 3001–3004, 1999.

Behera, S. K., and T. Yamagata, Influence of the Indian Ocean Dipole on the Southern Oscillation, *J. Meteorol. Soc. Jpn.*, *81,* l69–177, 2003.

Behera, S. K., S. A. Rao, H. N. Saji, and T. Yamagata, Comments on "A cautionary note on the interpretation of EOFs", *J. Clim.*, *16*, 1087–1093, 2003a.

Behera, S. K., J.-J. Luo, S. Masson, T. Yamagata, P. Delecluse, S. Gualdi, and A. Navarra, Impact of the Indian Ocean Dipole on the East African short rains: A CGCM study, *CLIVAR Exchanges, 27*, 43–45, 2003b.

Bjerknes, J., Atmospheric teleconnections from the equatorial Pacific, *Mon. Weather Rev., 97*, 163–172, 1969.

Black, E., J. Slingo, and K. R. Sperber, An observational study of the relationship between excessively strong short rains in coastal East Africa and Indian Ocean SST, *Mon. Weather Rev., 31,* 74–94, 2003.

Cadet, D. L., The Southern Oscillation over the Indian Ocean, *J. Clim.*, *5*, 189–212, 1985.

Cai, W., H. Hendon, and G. Meyers, Indian Ocean dipole-like variability in the CSIRO Mark 3 coupled climate model, *J. Clim.*, submitted, 2003.

Carton, J. A., G. Chepurin, X. Cao, and B. S. Giese, A simple ocean data assimilation analysis of the global upper ocean 1950–1995, Part 1: methodology, *J. Phys. Oceanogr., 30*, 294–309, 2000.

Chambers, D. P., B. D. Tapley, and R. H. Stewart, Anomalous warming in the Indian Ocean coincident with El Niño, *J. Geophys. Res., 104*, 3035–3047, 1999.

Clark, C. O., P. J. Webster, and J. E. Cole, Interdecadal variability of the relationship between the Indian Ocean Zonal Mode and East African coastal rainfall anomalies, *J. Clim., 16*, 548–554, 2003.

Clarke, A. J., and X. Liu, Interannual sea level in the northern and eastern Indian Ocean, *J. Phys. Oceanogr., 24*, 1224–1235, 1994.

Dommenget, D., and M. Latif, A cautionary note on the interpretation of EOFs, *J. Clim.*, *15*, 216–225, 2002.

Enomoto, T., B. J. Hoskins, and Y. Matsuda, The formation of the Bonin high in August, *Q. J. R. Meteorol. Soc., 587*, 157–178, 2003.

Feng, M., G. Meyers, and S. Wijffels, Interannual upper ocean variability in the tropical Indian Ocean, *Geophys. Res. Lett*., *28*, 4151–4154, 2001.

Fujiwara, M., K. Kita, S. Kawakami, T. Ogawa, N. Komala, S. Saraspriya, and A. Suripto, Tropospheric ozone enhancements during the Indonesian forest fire events in 1994 and 1997 as revealed by ground-based observations, *Geophys. Res. Lett., 26*, 2417–2420, 1999.

Gualdi, S., E. Guilyardi, A. Navarra, S. Masina, and P. Delecluse, The interannual variability in the tropical Indian Ocean as simulated by a CGCM, *Clim. Dyn., 20*, 567–582, 2003.

Guan, Z., K. Ashok, and T. Yamagata, Summer-time response of the tropical atmosphere to the Indian Ocean dipole sea surface temperature anomalies, *J. Meteorol. Soc. Jpn., 81*, 531–561, 2003.

Guan, Z., and T. Yamagata, The unusual summer of 1994 in East Asia: IOD Teleconnections, *Geophys. Res. Lett., 30,*

doi:10.1029/2002GL016831, 2003.

Guilyardi, E., P. Delecluse, S. Gualdi, and A. Navarra, The role of lateral ocean physics in the upper ocean thermal balance of a coupled ocean–atmosphere GCM*, Clim. Dyn., 17,* 589–599, 2001.

Hastenrath, S, A. Nicklis, and L. Greischar, Atmospheric–hydrospheric mechanisms of climate anomalies in the western equatorial Indian Ocean, *J. Geophys. Res., 98 (C11)*, 20219–20235, 1993.

Hastenrath, S., Dipoles, Temperature Gradient, and Tropical Climate Anomalies, *Bull. Am. Meteorol. Soc*., *83*, 735–738, 2002.

Hendon, H. H., Indonesian Rainfall Variability: Impacts of ENSO and Local Air–Sea Interaction, *J. Clim.*, *16*, 1775–1790, 2003.

Hoskins, B. J., On the existence and strength of the summer subtropical anticyclones, *Bull. Am. Meteorol. Soc.***,** *77*, 1287–1292, 1996.

Iizuka, S., T. Matsuura, and T. Yamagata, The Indian Ocean SST dipole simulated in a coupled general circulation model, *Geophys. Res. Lett*., *27*, 3369–3372, 2000.

Jury, R. M., Economic impacts of climate variability in South Africa and development of resource prediction models, *J. Appl. Meteorol.*, *41*, 46–55, 2002.

Jury, R. M., and B. Huang, The Rossby wave as a key mechanism of Indian Ocean climate variability, *Deep-Sea Res.,* submitted, 2003.

Kalnay, E., and coauthors, The NCEP/NCAR 40 year Reanalysis Project, *Bull. Am. Meteorol. Soc.***,** *77*, 437–471, 1996.

Klein, S. A., B. J. Soden, and N. C. Lau, Remote sea surface temperature variations during ENSO: Evidence for a tropical atmospheric bridge, *J. Clim.*, *12*, 917–932, 1999.

Lareef, Z., S. A. Rao, and T. Yamagata, Modulation of Sri Lankan Maha rainfall by the Indian Ocean Dipole, *Geophys. Res. Lett., 30*, doi:10.1029/2002GL015639, 2003.

Latif, M., and T. P. Barnett, Interactions of the tropical oceans, *J. Clim., 8*, 952–968, 1995.

Lau, N.-C., and M. J. Nath, Coupled GCM simulation of atmosphere–ocean variability associated with zonally asymmetric SST changes in the tropical Indian Ocean, *J. Clim.*, *17*, 245–265, 2004.

Li, C., and M. Mu, Influence of the Indian Ocean dipole on Asian monsoon circulation, *CLIVAR Exchanges*, *6*, 11–14, 2001.

Li, T., B. Wang, C.P. Chang, and Y. Zhang, A theory for the Indian Ocean Dipole–Zonal Mode, *J. Atmos. Sci.*, *60*, 2119–2135, 2003.

Luo J.-J., S. Masson, S. Behera, S. Gualdi, A. Navarra, P. Delecluse, and T. Yamagata, The updating and performance of the SINTEX coupled model on the Earth Simulator: Atmosphere part, *EGS Meeting, Nice, France*, 2003.

Madec, G, P. Delecluse, M. Imbard, and C. Levy, OPA version 8.1 ocean general circulation model reference manual, *Technical Report/Note 11*, LODYC/IPSL, *Paris, France*, pp 91, 1998.

Masson, S., J-P Boulanger, C. Menkes, P. Delecluse, and T. Yamagata, Impact of salinity on the 1997 Indian Ocean dipole event in a numerical experiment, *J. Geophys. Res.,* in press, 2003a.

Masson, S., J.-J. Luo, S. Behera, S. Gualdi, E. Guilyardi, A. Navarra, P. Delecluse, and T. Yamagata, The updating and performance of the SINTEX coupled model on the Earth Simulator: Ocean part, *EGS Meeting, Nice, France*, 2003b.

Masumoto, Y., and G. Meyers, Forced Rossby waves in the southern tropical Indian Ocean, *J. Geophys. Res., 103*, 27589–27602, 1998.

Meehl, G. A., The annual cycle and the interannual variability in the tropical Pacific and Indian Ocean regions, *Mon. Weather Rev.*, *115*, 27–50, 1987.

Meyers, G., Variation of Indonesian throughflow and El Niño–Southern Oscillation, *J. Geophys. Res*., *101*, 12255–12263, 1996.

Murtugudde, R. G., J. P. McCreary, and A. J. Busalacchi, Oceanic processes associated with anomalous events in the Indian Ocean with relevance to 1997–1998, *J. Geophys. Res*., *105*, 3295–3306, 2000.

Mutai, C. C., and M. N. Ward, East African rainfall and the tropical circulation/convection on intraseasonal to interannual timescales, *J. Clim.*, *13*, 3915–3939, 2000.

Nicholls, N., and W. Drosdowsky, Is there an equatorial Indian Ocean SST dipole, independent of the El Niño–Southern Oscillation? *Symp. on Climate Variability, the Oceans, and Societal Impacts*, Albuquerque, NM, Amer. Met. Soc., *17–18*, 2000.

Nitta, T., Convective activities in the tropical western Pacific and their impact on the Northern Hemisphere summer circulation, *J. Meteorol. Soc. Jpn., 65*, 373–390, 1987.

Ogallo, L., The spatial and temporal patterns of the East African seasonal rainfall derived from principal component analysis, *Int. J. Climatol., 9*, 145–167, 1989.

Perigaud, C., and P. Delecluse, Interannual sea-level variations in the tropical Indian Ocean from Geosat and shallow water simulations, *J. Phys. Oceanogr., 23,* 1916–1934, 1993.

Philander, S. G. H., Our Affair with El Niño, *Princeton Univ. Press*, in press, 2004.

Plumb, R.A., Three-dimensional propagation of transient quasi-geostrophic eddies and its relationship with the eddy forcing of the time-mean flow, *J. Atmos. Sci., 43*, 1657–1678, 1986.

Rao, S. A., S. K. Behera, Y. Masumoto, and T. Yamagata, Interannual variability in the subsurface tropical Indian Ocean with a special emphasis on the Indian Ocean Dipole, *Deep-Sea Res. II, 49*, 1549–1572, 2002a.

Rao, S. A, V. V. Gopalkrishnan, S. R. Shetye, and T. Yamagata, Why were cool SST anomalies absent in the Bay of Bengal during the 1997 Indian Ocean Dipole Event? *Geophys. Res. Lett*., *29*, doi:10.1029/2001GL014645, 2002b.

Rao, S. A., S. K. Behera, and T. Yamagata, Subsurface feedback on the SST variability during the Indian Ocean Dipole events, *Dyn. Atmos. Ocean,* submitted, 2004.

Rayner, N. A., E. B. Horton, D. E. Parker, C. K. Folland, and R. B. Hackett, *Clim. Res. Tech. Note, 74*, UK Met. Office, Bracknell, 1996.

Rodwell, M. J., and B. J. Hoskins, Monsoons and the dynamics of deserts, *Q. J. R. Meteorol. Soc., 122*, 1385–1404, 1996.

Roeckner, E., and coauthors, The atmospheric general circulation model ECHAM4: model description and simulation of present day climate, *Max Plank Institute fur Meteorologie Rep., 218*, Hamburg, Germany, pp90, 1996.

Ropelewski, F., and M. S. Halpert, Global and regional scale precipitation patterns associated with the El Niño /Southern Osicllation, *Mon. Weather Rev.*, *115*, 1602–1626, 1987.

Saji, N. H., B. N. Goswami, P. N. Vinayachandran, and T. Yamagata, A dipole mode in the tropical Indian Ocean, *Nature, 401*, 360–363, 1999.

Saji, N. H., and T. Yamagata, Structure of SST and surface wind

variability during Indian Ocean Dipole Mode events: COADS observations, *J. Clim., 16*, 2735–2751, 2003a.

Saji, N. H., and T. Yamagata, Possible impacts of Indian Ocean Dipole Mode events on global climate, *Clim. Res.*, *25*, 151–169, 2003b.

Sardeshmukh, P. D., and B. J. Hoskins, The generation of global rotational flow by steady idealized tropical divergence, *J. Atmos. Sci*., *45*, 1228–1251, 1988.

Shinoda, T., M. A. Alexander, and H. H. Hendon, Remote response of the Indian Ocean to interannual SST variations in the tropical Pacific, *J. Clim.*, in press, 2003.

Takaya, K., and H. Nakamura, A formulation of a phase-independent wave-activity flux for stationary and migratory quasigeostrophic eddies on a zonally varying basic flow, *J. Atmos. Sci., 58*, 608–627, 2001.

Tourre, Y. M., and W. B. White, ENSO signals in the global upper-ocean temperature, *J. Phys. Oceanogr.*, *25*, 1317–1332, 1995.

Tozuka, T., and T. Yamagata, Annual ENSO, *J. Phys. Oceanogr.*, *33*, 1564–1578, 2003.

Ueda, H., and J. Matsumto, A possible trigerring process of east–west asymmetric anomalies over the Indian Ocean in relation to 1997/98 El Niño, *J. Meteorol. Soc. Jpn., 78*, 803–818, 2000.

Valcke S., L. Terray, and A. Piacentini, The OASIS coupler user guide version 2.4, *Technical Report TR/CMGC/00-10*, CERFACS, Toulouse, France, pp 85, 2000.

Venzke, S., M. Latif, and A. Villwock, The coupled GCM ECHO-2. Part II: Indian Ocean response to ENSO*, J. Clim., 13*, 1371–1383, 2000.

Vinayachandran, P. N., N. H. Saji, and T. Yamagata, Response of the equatorial Indian Ocean to an anomalous wind event during 1994, *Geophys. Res. Lett*., *2*6, 1613–1616, 1999.

Vinayachandran, P. N., S. Iizuka, and T. Yamagata, Indian Ocean Dipole mode events in an ocean general circulation model, *Deep-Sea Res. II, 49*, 1573–1596, 2002.

Wang, B., and Z. Fan, Choice of South Asian summer monsoon indices, *Bull. Am. Meteorol. Soc., 80*, 629–638, 1999.

Webster, P. J., A. Moore, J. Loschnigg, and M. Leban, Coupled ocean–atmosphere dynamics in the Indian Ocean during 1997–98, *Nature, 40*, 356–360, 1999.

White, W. B., Coupled Rossby waves in the Indian Ocean on inter-annual time scales, *J. Phys. Oceanogr., 30*, 2972–2989, 2000.

Willmott, C. J., and K. Matsuura, Smart interpolation of annually averaged air temperature in the United States, *J. Appl. Meteorl*., *34*, 2557–2586, 1995.

Xie, S.-P., H. Annamalai, F. Schott, and J. P. McCreary, Structure and Mechanisms of south Indian Ocean climate variability, *J. Clim.*, *15*, 864–878, 2002.

Yamagata, T., S. K. Behera, S. A. Rao., Z. Guan, K. Ashok, and H. N. Saji, The Indian Ocean dipole: a physical entity, *CLIVAR Exchanges, 24***,** 15–18, 2002.

Yamagata, T., S. K. Behera, S. A. Rao, Z. Guan, K. Ashok, and H. N. Saji, Comments on "Dipoles, Temperature Gradient, and Tropical Climate Anomalies", *Bull. Am. Meteorol. Soc., 84*, 1418–1422, 2003.

Yule, G. U., On the Theory of Correlation for any Number of Variables, Treated by a New System of Notation, *Proc. Royal Soc. Series A, 79*, 182–193, 1907.

S. K. Behera, J.-J. Luo, S. Masson, S. A. Rao, and T. Yamagata, Frontier Research System for Global Change, Yokohama, Kanagawa 236–0001, Japan. (yamagata@eps.s.u-tokyo.ac.jp)

M. R. Jury, Environmental Science Department, University of Zululand, South Africa.